THE CRYSTALLIZATION KINETICS OF POLYETHYLENE IN EXTENSIONAL DEFORMATION

By

SHENG MA

Bachelor of Science

Zhejiang University

Hangzhou, People's Republic of China

1990

Submitted to the Faculty of the
Graduate College of the
Oklahoma State University
in partial fulfillment of
the requirements for
the Degree of
MASTER OF SCIENCE
December, 1994

THE CRYSTALLIZATION KINETICS OF POLYETHYLENE

IN EXTENSIONAL DEFORMATION

Thesis Approved:

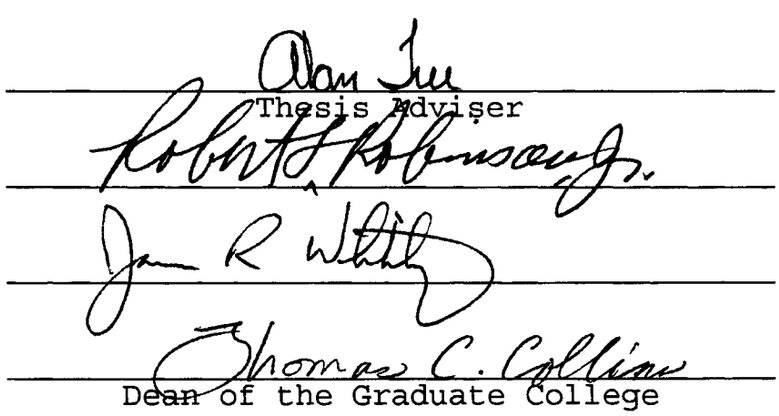

Thesis Adviser

Dean of the Graduate College

ACKNOWLEDGMENTS

I wish to express my sincere gratitude to my major advisor, Dr. D. Alan Tree, for his guidance, encouragement, interest and valuable suggestions. Gratitude is also extended to the other committee members, Drs. J. R. Whiteley and Robert L. Robinson, Jr.

I wish to thank Tsung-Chieh Tsai and Xiao-Feng Guan for their help with the experiment and computers.

I also would like to express my gratitude to my parents and my sister for many sacrifices, continuous support, much understanding and love, and never-ending patience throughout the course of this endeavor.

TABLE OF CONTENTS

Chapter Page

LIST OF TABLES

LIST OF FIGURES

Figure Page

LIST OF SYMBOLS

Symbol

A	Cross section area of sample
C	Stress optic coefficient
D	Thickness of sample
d	Thickness of sample
d_0	Initial thickness of sample
HDPE	High density polyethylene
I	Intensity of transmitted light
I_0	Intensity of incident light beam
K_d	Proportionality constant
L	Thickness of sample
N	Number of non-activated crystallization sites
r	Radius of roller
T_r	Torque acting on sample
t	Time
v	Volume of a crystal
w_0	Initial width of sample
w	Width of sample
z	Past time
ϕ	Volume fraction of crystal at a given time
ϕ_∞	Volume fraction of crystal obtained at infinity time
λ	Wave length of light

Symbol

η_{p1}	First principal refractive index
η_{p2}	Second principal refractive index
χ_M	Orientation angle of the stress tensor
χ_o	Orientation angle of the refractive index tensor
χ	Isoclinic angle
Δ	Birefringence
τ_{p1}	First principal stresses
τ_{12}	Shear stress
α	Polarizer orientation angle
ϵ	Strain rate
δ_a	Retardation of amorphous carrier phase
δ_d	Retardation of amorphous sample phase
δ_c	Retardation of crystalline regions of sample
δ_{tot}	Total test section retardance
$\delta_{da,0}$	Sample amorphous retardation on cessation of flow
θ	Temperature dependent relaxation time

CHAPTER I

INTRODUCTION

Polymer materials are becoming increasingly important in our lives. Metals, glasses and natural fibers are being replaced by polymeric materials because polymers are tougher, more flexible, less expensive, and resistant to corrosion. Carefully processed polymeric materials have drawn considerable attention because of the improved mechanical and physical properties.

Polymeric materials generally have relatively poor mechanical strength, eventhough the carbon-carbon covalent bond in a polymer chain is very strong. In the melt or solution, polymer molecules prefer to exist in the random coil configuration. If the molten or solute polymer molecules is under the influence of a stress field, molecules can be induced to extend and orient. When crystallization occurs under these conditions, the molecules will often form extended chain crystals. If the stress field is generated by a flow field, the process is called flow-induced crystallization (FIC) (1). To produce polymer products with superior mechanical properties, controlling the processing conditions is critical. For example,

commonly processed polyethylene is relatively weak, however, polyethylene fibers or drawn gel polyethylene fibers show a dramatic increase in mechanical properties. The increased tensile modules and breaking strength are due to the presence of extended chain crystals, thus demonstrating the potential of flow-induced crystallization to produce high strength, stiff polymer materials.

Full exploitation of flow-induced crystallization requires a knowledge of the crystallization kinetics. However, the current applications of flow-induced crystallization involve large, non-homogeneous extension rates; sudden, large temperature drops; and solvent mass transfer which make kinetic measurements very difficult. Developing a means to overcome the experimental difficulty is very important.

To study flow-induced crystallization, equipment to produce an uniform extensional flow at constant temperature is needed, which also allows for the measurement of the stress, strain, and degree of crystallinity. The purpose of this study is to develop a means to overcome the experimental difficulties and generate kinetic data of flow-induced crystallization in extensional flow. The experiment described in this thesis meets all of the requirements for the study of flow-induced crystallization kinetics.

The remainder of this thesis is divided into four chapters. Chapter II contains the relevant background and theoretical development for flow-induced crystallization.

Chapter III presents the details of the equipment and experimental techniques. Chapter IV presents the data and a discussion of the results. Chapter V presents the conclusions and recommendations.

CHAPTER II

BACKGROUND

An understanding of flow-induced crystallization kinetics requires the knowledge of several subjects including: the history of flow-induced crystallization, extensional flow, polymer crystallization theory and birefringence. Only the studies that are central to this work have been reviewed in this chapter. More intensive reviews have been given by Tree (1) and Siddiquee (23).

Flow-Induced Crystallization

The first report of flow-induced crystallization from the melt was by van der Vegt and Smit (2) in 1967. Van der Vegt and Smit observed a dramatic increase in the pressure when an isotactic polypropylene melt was extruded through a capillary die at a temperature just above the melting point. Eventually the pressure became so great that no flow was possible. X-ray diffraction patterns of the material from inside the die revealed that the polymer molecules were highly oriented in the direction of the flow. Van der Vegt and Smit proposed that the molecules had been aligned in the extensional flow field near the entrance to the capillary

and subsequently crystallized in the capillary. The crystallization resulted in die blockage which caused the pressure rise and the abrupt end of the experiment.

The results of van der Vegt and Smit were confirmed by Seigloff and O'Leary in 1968 (3,4) and Southern and Porter in 1970 (5,6). However, there was no provision for in-situ observation of the flow-induced crystallization. In one case (7), the use of robust die designs has enabled in-situ observations of the solidification process during continuous extrusion of self-reinforced polyethylene and polypropylene films; however, quantitative analysis of the crystallization kinetics was not possible.

Considerable work has been done by Tsebrenko and Vinogradov (8) on the flow-induced morphology of incompatible polymer blends. Tsebrenko and Vinogradov introduced a two phase flow in which the minor phase formed fibrils in the matrix of the carrier phase. In the capillary experiment, the suspended droplets of the minor phase were relatively undistorted in the die; however, near the entrance to the capillary the suspended droplets were drawn out into fibrils by the action of the extensional flow. Tree and McHugh (9,10) realized that the fibrillation mechanism was caused by the same extensional kinematics flow that produced flow-induced crystallization at the entrance to the capillary in the van der Vegt and Smit experiments.

G. Titomanlio and G. Marrucci (11) further investigated the behavior of HDPE in the capillary apparatus.

Capillaries of various lengths were used to change the relative importance of shear with respect to elongation. Also, the effect of changing the capillary length, which gave different pressure drops, was investigated. The results showed that flow-induced crystallization in a capillary is a complex phenomenon where both the elongational flow at the entrance and the shear flow along the capillary play substantial roles.

Ness and Liang (12) also found that the shear-induced crystallization was easily produced using a capillary rheometer when the temperature was near the melting point of the samples, even though the shear rate was not high.

The most significant work on flow-induced crystallization in extensional flow has been done by McHugh and his coworkers (7,9,10,13-22,35). Tree and McHugh (9,10), as mentioned above, studied the extrusion of two phase polymer blends consisting of a Linear Low Density Polyethylene as the major or carrier phase and small amounts of a crystallizable polymer as the minor or suspended phase. Extended chain crystallinity was induced in the minor phase without the die blockage problem. However, rheological measurements were insufficient for detecting crystallization.

Sakellarides and McHugh (13) constructed a slit flow die with optical windows which was used to extrude polymer blends. The optical windows allowed for in-situ observation of flow-induced crystallization for the first time. This

work demonstrated that in shearing flow, polymer droplets deform by emitting "tails" from the upstream and downstream ends and that flow-induced crystallization occurs inside the tails. Sakellarides developed a model of tail growth as a function of time and showed that the flow inside the tails could be extensional if the two phase blend had the proper viscosity ratio.

The first report of quantitative flow-induced crystallization kinetic data in extensional flow was by Tree (1). In his experiments, a molten droplet of a crystallizable polymer phase was suspended in a second non-crystallizing phase while the system was subjected to an extensional flow field. The flow field was generated by a 4-Roll Mill device. Optical windows in the 4-Roll Mill allowed birefringence measurements in both the droplet and carrier phases. From the birefringence measurements, the carrier phase stress fields and the crystallization rates within the droplet were calculated as a function of time and position.

Guy (14) continued Tree's work with the 4-Roll Mill and video image techniques. Guy demonstrated the importance of accounting for dichroism. Guy also introduced a simplified data analysis which was made possible by collecting data upon cessation of flow instead of during the flow. The initial growth rate shows a dependence on both the macroscopic orientation and strain experienced during the deformation preceding crystallization which can not be

explained quantitatively or qualittively by the melting point elevation model. A minimum orientation or strain level is also necessary to induce oriented crystallization.

Guy's data showed that the change in crystallization rate with temperature is less dramatic than one would expect for a nucleation controlled process while the crystal growth rate is much greater than in the quiescent state.

Extensional Flow

A tremendous amount of work has been done to produce uniaxial extensional flows to orient and crystallize flexible-chain polymers. However, this work has focused primarily on temperatures well below T_m. Tree (1) and Siddiquee (23) have given very intensive reviews on the development of devices which produce extensional flow fields. The studies after 1992 have been reviewed in this section.

The experimental work of Elyasherich et al. (24) involved preparation and studying of melt extruded films and fibrillated films (obtained by pressing and quenching of films) of linear polyethylene formed by two techniques, ie. crystallization initiated by melt extension and uniaxial stretching of a crystallized polymer. The grains of high density polyethylene were melted in an extruder. To prepare the melt for crystallization, a tempering two-drum unit was used. The polymer from the extruder reached the drums at a

temperature in the region of crystallization. After leaving the drums, the polymer was drawn by a pair of rolls to the desired draw ratio. Elyasherich and his coworkers found that orientational crystallization takes place in an extremely narrow temperature region, and processing using the drawing technique had a good stability.

Salem (25,26) studied the evolution of crystallinity during the uniaxially drawing of poly (ethylene terephthalate) on an Instron tensile tester at 90 °C and at strain rates in the range 0.01-0.25 s^{-1}. The amorphous film specimen was mounted on the jaws of an Instron tensile tester and drawn at the selected extension rate. Wide-range X-ray scattering analysis with a Phillips diffractometer in the transmission mode was used in the experiment. Salem found there is a precrystallization regime involving deformation of an entanglement network, followed by two crystallization regimes which significantly influence stress-strain behavior: the low stress crystallization regime involving the formation of a crystallite network and a high stress crystallization regime involving growth of crystallites and deformation of a network. For the constant extension rate experiment, Salem found that crystallinity could almost be considered as a single function of true stress, with little influence of the strain rate.

Pazur et al. (27) characterized the crystalline and amorphous orientation of a uniaxially deformed low-density polyethylene (LDPE) film combined with pole figure X-ray

diffraction and birefringence measurements. The drawing was carried out in an Instron tensile tester. Pazur reported that at small draw ratios ($\lambda < 1.04$), the amorphous regions remained biaxially oriented. However, at slightly higher elongations ($\lambda > 1.12$), the amorphous regions slowly acquired a uniaxial orientation. Pazur tried to quantify the induced orientation by Hermans, Normara/Kawai and White/Spruiell orientation functions. However, all quantifications by orientation functions were hindered by the presence of orientation populations which had to be deconvoluted and analyzed separately.

The development of orientation has been studied by Voice et al., (28,29) in a sample of poly (aryl ether ether ketone) (PEEK). Uniaxial drawing was performed on an Instron tensile testing machine at 150 °C from an initially amorphous state at an initial strain rate of 40% min^{-1}, which produced films that were both evenly drawn and had high orientation. Draw ratios in the range of 1 to 3.24 were obtained for the thick films (300 μm). Refractive index and X-ray measurements were made on the samples. The polarized spectra was also used in the experiment. Voice et al. (28,29) found that the development of molecular orientation in PEEK was probably a pseudo-affine process modified by crystallization. Finally Voice et al. (29) concluded that at temperatures slightly above the glass-transition temperature (T_g), very few crystals were formed before the draw ratio reached 2. As a draw ratio of

approximately 2 is reached, "the crystallinity begins to increase much more rapidly because the molecules are so well aligned that they can fall into crystal register" (29).

Kaito et al. (30) studied the structure formation in stretched poly (butylene terephthalate) (PBT) sheets as a function of draw ratio, drawing temperature, and the crystallinity of the original sample. The results showed the crystallinity is sensitive to the temperature and increased with increasing draw ratio.

The molecular orientation, induced crystallization, and mechanical properties of amorphous poly (ethylene terephthalate) (PET) stretched at different temperature and strain rates were studied by Chang et al. (31). The extension of the specimen was performed in a hot-air oven by an Instron tensile testing machine under constant temperature and strain rates. The orientation of PET was found to vary strongly with both temperature and strain rate; however, the strain-induced crystallinity seems to be dependent on temperature only. A rubber network model was used to give a quantitative description of the development of orientation with draw ratio.

As cited above, tremendous effort have been made to measure the extensional flow-induced crystallization kinetic data. However, due to the difficulty of the experimental work and unsatisfactory experimental devices, there are no quantitative kinetic data obtained except for those presented by Tree (1) and Guy (14). Therefore, the

development of an experimental device that can generate an extensional flow in a polymer melt; allow for the easy measurements of stress, strain rate; maintain a constant temperature and combine with an optical technique to obtain the flow-induced crystallization kinetic data is very important.

Meissner (32) developed an apparatus called the Universal Extensional Rheometer (UER) for the uniaxial extension of polymer melts. The report on his first version of the equipment was published in 1969. The UER consisted of two rotary clamps at a specified distance from each other and driven by synchronous motors. A polymer melt sample, floating on silicon oil, could be elongated at a constant strain rate. In subsequent versions, temperature control was improved. In the final version, UER-1 (model 4), one of the motors was located and operated under silicon oil at temperatures up to 200 °C. The sample could be elongated at a desired Hencky strain rate and the stress acting on the sample could be measured. The development of the UER provided the opportunity for studying extensional flow-induced crystallization because of the simple operation process, easy stress and strain measurements, and accurate temperature control.

Siddiquee (23) modified the Meissner Rheometer by combining the rheometer with the optical techniques of Tree and McHugh (1). The modified Meissner Rheometer is described in much greater detail in Chapter III and was used

in the experiments described in Chapter IV.

Crystallization Kinetics

Most of work done to model flow-induced crystallization has been based on the Avrami theory. Avrami (1,33) considered the readily observed case in which grains of a polymer crystal grow from activated, discreet nucleation sites such as dust or catalyst remnants under quiescent, isothermal conditions and where the crystals have unlimited volume in which to grow. The Avrami approach assumes that crystallization site becomes activated over time and then grow at some constant rate. The total volume of crystal is then given as the sum of the volume of crystal at each crystallization site.

However, the Avrami theory could not account for the effects of stress, strain and orientation during flow-induced crystallization process. Considerable work has been done to modify the theory by considering the effects of stress, strain and flow factors (1, 34,35). Tree (1) introduced the stress and flow factors into the Avrami theory to account for the effects of stress and flow field. Tree considered that the flow-induced crystallization could be a function of stress.

Desai et al. (34) suggested a framework to allow the nucleation rate to be a function of precrystalline orientation. However, no indication of the dependency of nucleation rate on orientation was reported.

A melting point elevation model was also often used to explain flow-induced crystallization (35). This argument is based on the Gibb's Free Energy Expression:

$$\Delta G = \Delta H - T\Delta S \qquad (1)$$

where:

ΔG = change in Gibb's Free Energy

ΔS = change in entropy

ΔH = change in enthalpy

T = temperature.

When crystal form, the change of Gibb's Free Energy is equal to zero, so:

$$T_m = \frac{\Delta H}{\Delta S} \qquad (2)$$

where: T_m = melting point temperature.

The melting point elevation model proposed that when polymer molecules were stretched under flow, the change of entropy from oriented molecules to extended chain crystal is less than the change of entropy from random oriented molecules to a folded chain crystal. The model also suggested that the change of enthalpy for both process are the same. Thus, leading to an elevation in melting point temperature. However, the kinetic data obtained by Tree (1) and Guy (14) showed the melting temperature was completely unaffected during the process of flow-induced

crystallization. The structure of folded chain crystals and extended chain crystals showed that the molecules of folded chain crystal and extended chain crystal exist in the same configuration. The molecules are all aligned parallel to each other in both type of crystals except for the molecules at the folds of the folded chain crystals.

Guy (14) noted that the initial growth rate showed a dependence on both the macroscopic orientation and strain experienced during the deformation preceding crystallization. He suggested a type of visco-elastic, molecular strain due to flow-orientation may be the controlling process for the flow-induced crystallization. However, due to lack of kinetic data, no complete quantitative model has been developed for the flow-induced crystallization. Further experimental data are needed to develop a successful model for this important process.

Flow Birefringence

The first systematic studies of birefringence in polymeric system were performed on solutions of natural and synthetic polymers in 1930 by Von, Edsall and Signer (36,37). Birefringence is the difference in the refractive indices along the two principle axes of a material which cause a beam of polarized light to split into two beams (the ordinary and extraordinary beams) which travel along these axes at different speeds. Generally, most molecules are optically anisotropic. When the molecules in an assembly

are completely randomly distributed, the assembly behaves as an isotropic medium. If the assembly can be brought either partially or fully into a state of orientation, birefringence may occur. Birefringence can be used to quantify the level of orientation in a transparent polymer. During drawing of a crystallizable polymeric material, its birefringence increases as a consequence of chain orientation and extended chain crystals in the direction of stress. For a better understanding of flow birefringence, the development of the technique is briefly described which closely follows the presentation of Tree (1).

A beam of polarized light in the material can been envisioned as splitting into two beams which travel along the two principal optical axes at different speeds. The relative phase difference, R, due to the different rate of propagation of the emerging beams is given by

$$R = \frac{L}{\lambda}[\eta_{p1} - \eta_{p2}] \qquad (3)$$

where

L = thickness of the medium

λ = wave length of the light

η_{p1} = first principal refractive index

η_{p2} = second principal refractive index

$\eta_{p1}-\eta_{p2}$ = birefringence.

Closely related to the phase difference, R, is the retardance, δ, which is given by: $\delta = 2\pi R$.

The values of Δ (birefringence) at a given point in a flow can be determined by the use of a plane polariscope. The plane polariscope consists of a light source, a collimating lens, a monochromatic filter, the sample and a second polarizer. The expression for the fraction of transmitted light, T, as a function of the birefringence and isoclinic angle, at a given point is given by Equation (4) which was developed by Tree (1):

$$T = \frac{1}{4}\sin^2\left(\frac{\pi L \Delta}{\lambda}\right)[1 - \cos 4(\chi - \alpha)] \qquad (4)$$

where

L = the sample thickness

λ = the wave length of light

α = the polarizer orientation angle

χ = the isoclinic angle.

The angle α is measured from an arbitrary reference direction. Usually the reference direction is taken as χ = 0. In the above equation the "$\sin^2$" part is called the isochromatic term and the "cos" part is called the isoclinic term. Total extinction can be reached if either the isoclinic or the isochromatic term is zero.

When working on semicrystalline polymeric systems, birefringence can be expressed in terms of the equation derived by Stein (38):

$$\Delta n = \Delta n_c + \Delta n_a + \Delta n_f + \Delta n_d \quad (5)$$

where

Δn_c = the intrinsic birefringence of the crystalline regions

Δn_a = the intrinsic birefringence of the amorphous phases.

Δn_f = the form birefringence

Δn_d = the deformation birefringence.

Experiments of flow-induced crystallization combined with the birefringence technique have been reported by many investigators (39, 40-42). Tree (1) used the technique of video imaging in conjunction with the measurement of the birefringence in his experiment and obtained the extensional flow-induced crystallization kinetic data for the first time.

Summary

Since Van der Vegt and Smit first reported the flow-induced crystallization phenomena. Many investigator have tried to overcome the experimental difficulties to generate extensional flow-induced crystallization kinetic data. However, the investigators were all been hindered by experimental difficulties. Now, data on the nucleation and growth kinetics in sheared melts are available, but measurements of extensional flow-induced crystallization are virtually non-existent. This is because extensional flow-

induced crystallization is so sensitive to small flow and temperature variations that it is hard to control, and because of the excessive pressure gradients and eventually flow blockage due to massive crystallization.

Tree (1) and Guy (14) generated the first in-situ, quantitative data of flow-induced crystallization process. However, the data obtained were limited and the work was tedious due to the difficulty of the experiment.

Therefore, to create an experimental apparatus and technique that can solve the problem of controllability and flow blockage in the experiment is very important. The experiment requires that the orientation levels can be unambiguously determined by in-situ visualization, and the transformation kinetics can be analyzed based on a property that can be measured unobtrusively and which is directly related to the crystallization, and can obtain the kinetic data over a wider range in extension rate and in a relatively easier way than that previously reported.

CHAPTER III

EXPERIMENTAL APPARATUS AND TECHNIQUES

The experimental work was aimed at understanding the crystallization kinetics of polyethylene in extensional deformation via analysis of birefringence and torque data. In order to accomplish the goal of our experimental work, a modified Meissner Rheometer was used and new experimental techniques were developed. This chapter contains a detailed description of the experimental apparatus, techniques and procedures.

A flow-diagram of the experimental setup is shown in Figure 1. The required extensional flow field was generated by a modified Meissner Rheometer. A data logging system was used to record the torque acting on the polymer sample. An optical set up was used to produce birefringence patterns. Birefringence behavior was recorded by a VCR and analyzed by computer software.

Meissner Rheometer

The modified Meissner Rheometer, as shown in Figure 2, consists of two pairs of rotary clamps (labeled A, B and C, D) made from stainless steel and stainless steel shafts.

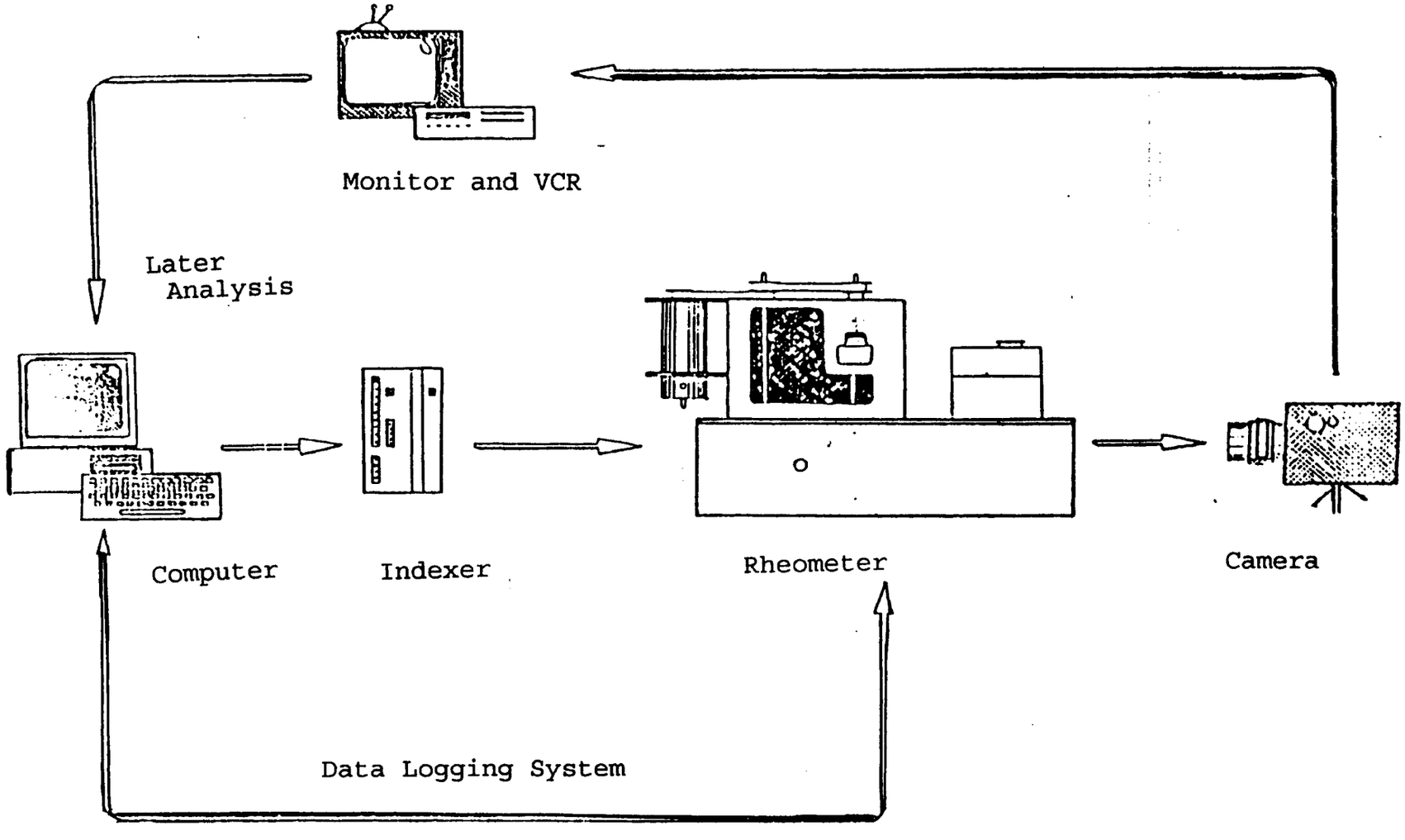

Figure 1. The Flow Diagram of the Experimental Setup

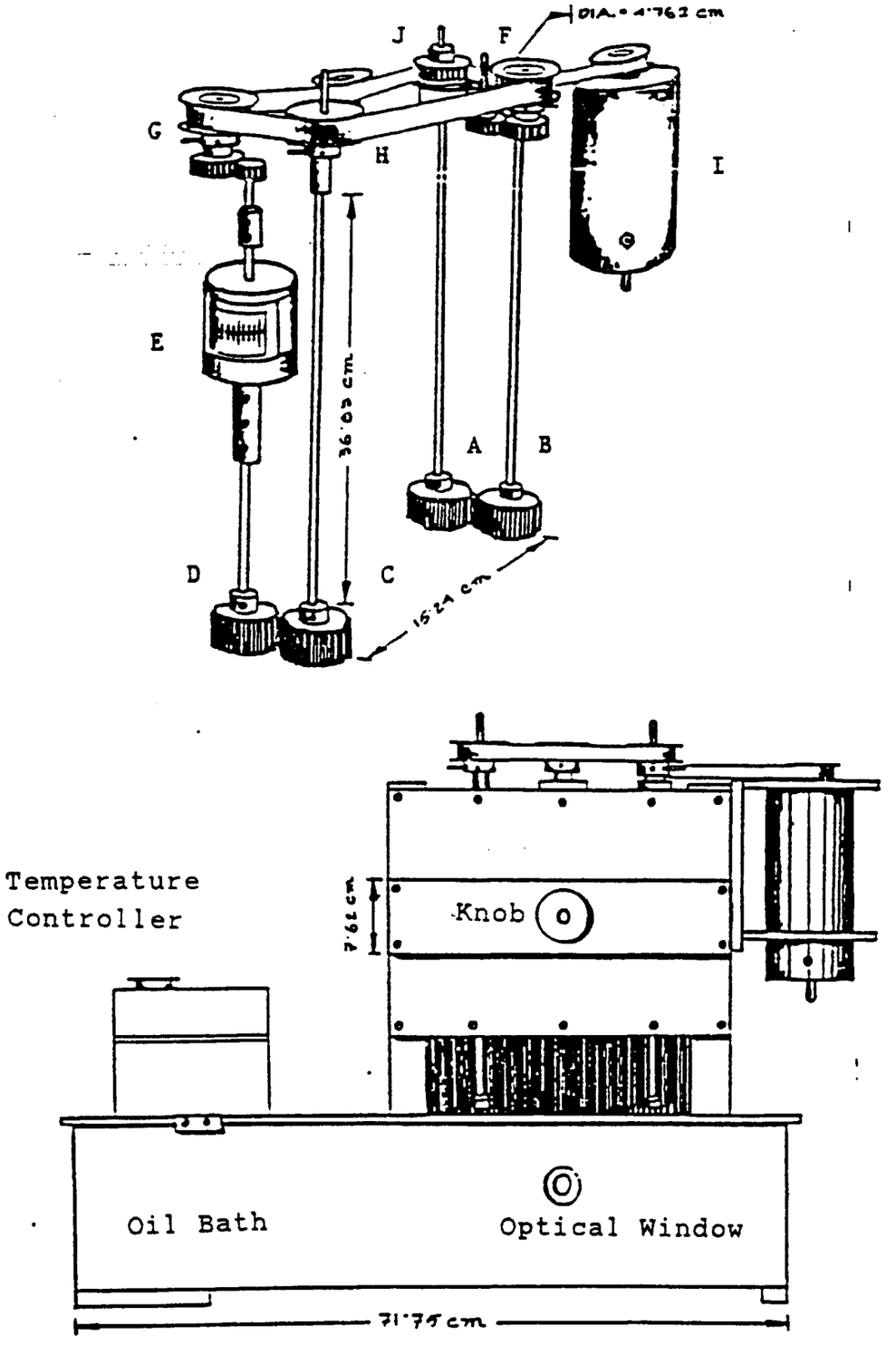

Figure 2. The Modified Meissner Rheometer (23)

Rollers were screwed to the shafts. The other end of the shafts were connected to the rotation mechanism. The rotation mechanism consisted of pulleys, idler shafts and timing belts (parts F through H and J). One of the pulleys was driven by a computer controlled motor (part I). The arrangement kept each roller at the same rotation rate while allowing adjacent rollers to rotate in the opposite direction.

The four rollers with the polymer sample were immersed in a temperature controlled oil bath with a stainless steel liner. There were two round optical windows located at the front and back of the bath, through which the birefringence pattern was observed and recorded during the experiment.

Silicon oil was used as the heating medium in the temperature bath, and a temperature controller from Techne (Model TU-16A) was used to maintain a uniform temperature to within ± 0.5 °C.

The extensional flow field was generated by stretching the two ends of the molten polymer sample at a constant extensional rate. The constant extension rate was produced by rotating the rollers. The motor was connected to the computer and programmed to a desired velocity through X-language commands.

Data Logging System

In Siddiquee's experiment (23), the torque acting on the sample was recorded with a strip chart recorder. The

arrangement made the experimental work very tedious and introduced significant errors. In order to obtain the torque data more easily and precisely, a data logging system was set up to record the torque acting on the polymer sample during the flow and after the cessation of flow. The data logging system included a Cole-Parmer #08109-25 (model 14c) analog interface card that enables an IBM PC to translate analog voltages into digital equivalents (3 data points per second), and a flexible general purpose data acquisition package, Cole-Parmer #08109-32 (PC64). The data could be displayed on the screen and logged or charted on a printer.

Optical and Video Set Up

Proper optical and video set ups were very important for the acquisition of the birefringence data. The optical set up, shown in Figure 3, was the same as Siddiquee used in his experiments (23). The optical path consisted of a light source, a collimating lens, a light filter, a polarizer, the polymer sample and an analyzer.

The light source was an Earling Fiber Optics System with a light pipe. The emission end of the pipe was covered with foil and pricked with a needle to give a good approximation of a point source of light. The light filter had maximum transmission at 488 nm (blue light). The polarizer and analyzer had a clear aperture of 9.6 cm when mounted. All of the elements of the optical train were mounted in their respective holders except for the polymer

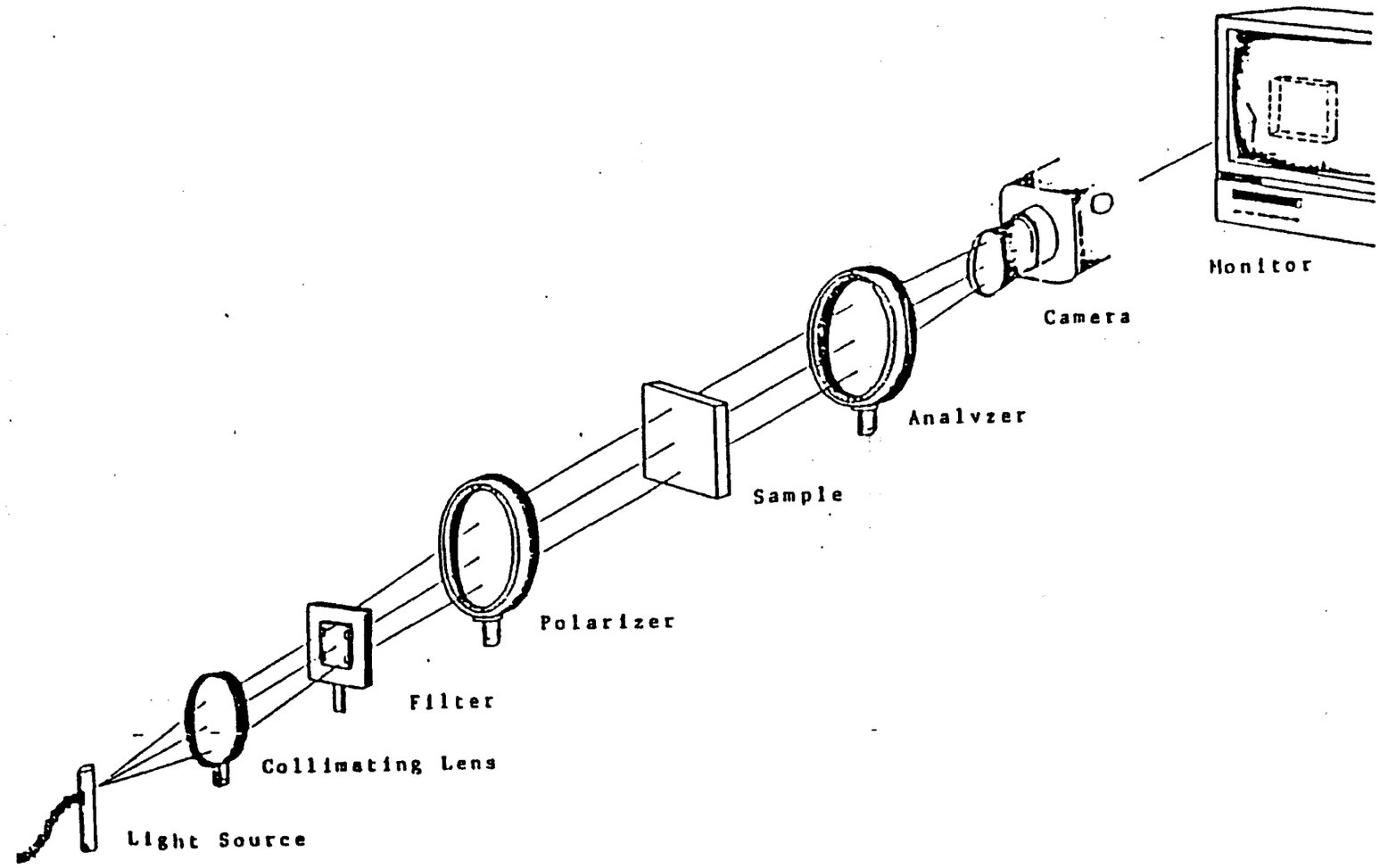

Figure 3. Optical Set Up (23)

sample which was immersed in the silicon oil. The optical holders were clamped to a aluminum optical rail.

A video set up, as shown in Figure 4, was used to monitor and record the birefringence pattern during the experiment. The video set up consisted of a black and white video camera (30 frames/sec.), a VCR, and a black and white monitor. The video camera and VCR were used to record the birefringence behavior. A monitor was used to view the birefringence pattern during the experiment and also to analyze the data. The video camera was set on the tripod in front of the equipment and set at the same height as the optical window of the temperature bath. To assure that the light through the window was horizontal, the oil bath and the optical rail were leveled with a spirit level. The light source was adjusted horizontally and vertically to appear in the center of the monitor. The light source was adjusted so that the maximum pixel value was less than 255.

Sample Preparation

Polymer samples used in the experiment were high density polyethylene from Quantum Chemical Corporation. Selected physical property data are listed in Table I. A smooth, homogeneous polymer sample was needed for the experiment. Siddiquee (23) used samples extruded in 2.54 cm (1.0 in.) by 0.317 cm (0.125 in.) strips at 160 °C. The polymer samples obtained by this method were often wavy and bent at the edges. Therefore, an improved technique was

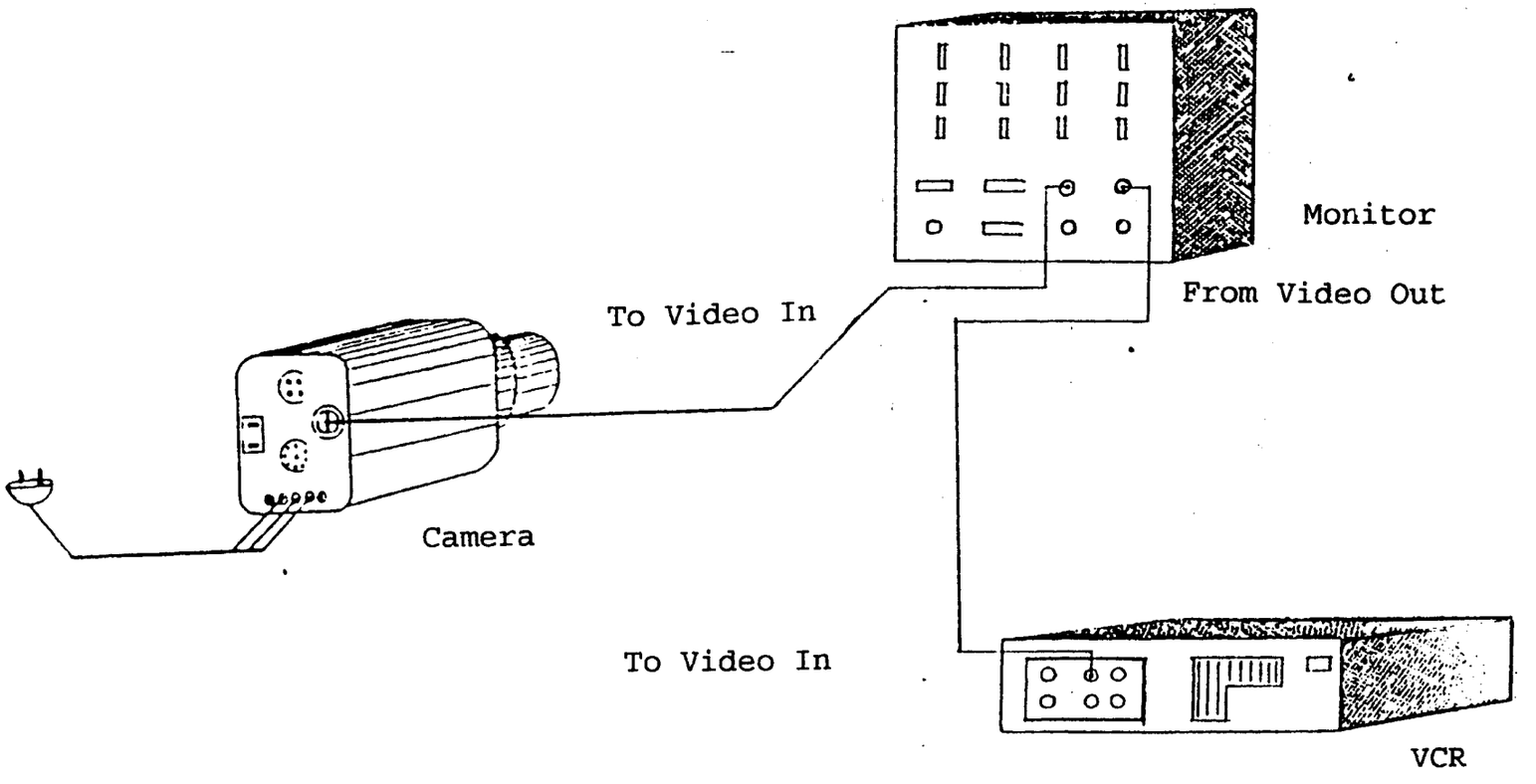

Figure 4. Wiring Diagram: Connection Among the Camera, the Monitor and the VCR (23)

TABLE I

Physical Properties of High Density Polyethylene (Quantum Chemical Corporation LS 6601-00) (49)

Property	Nominal Value	Units	ASTM Test Method
Density	0.952	g/cm^3	D 1505
Melt Index	6.5	g/10 min.	D 1238
Tensile Strength	4,000	psi	D 638
Elongation @ Break	400	%	D 638
Flexural Modules	160,000	psi	D 790
Tensile Impact	27	ft-lb/in.	D 1822
Low Temp. Brittleness	< -76	°C	D 746
Vicat Softening Point	125	°C	D 1525
Hardness, Shore D	66		D 2240

used to produce polymer samples with homogeneous properties.

An aluminum die, shown in Figure 5, was used to compression mold the polymer resin and produce the polymer sample. The bottom half of the die had a cavity 19.4 cm long, 2.54 cm wide and 0.25 cm deep to produce the sample. The die was designed to produce a smooth, homogeneous polymer sample. Compared to the method Siddiquee (41) used, the die solved the problem of inhomogeneous, bent, and wavy samples. Before the polymer resin was put in the die cavity, the surface of the die was coated with silicon oil to prevent the molten polymer from sticking to the die. The bottom half of the die was filled with polymer, in the form of pellets, and heated to 160 °C in a vacuum oven to remove any air bubbles. After six hours, the die was removed from the oven and checked for air bubbles in the polymer melt. Before the die was closed and pressure was applied, a piece of paper was placed between the two parts of the die to prevent bubbles from forming during the process. Pressure was then applied on the die using a Carver Laboratory Press at 160 °C for 30 minutes to remove the stress inside the sample. After 30 minutes, the die was allowed to cool, and the sample was removed and checked for air bubbles and voids. Any sample containing a void was rejected.

Techniques and Procedure

The first step in the experimental work was to calibrate the data logging system.

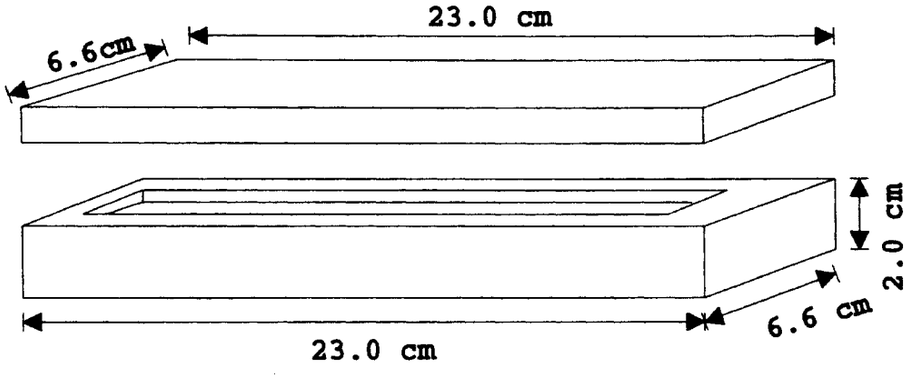

Pictorial View

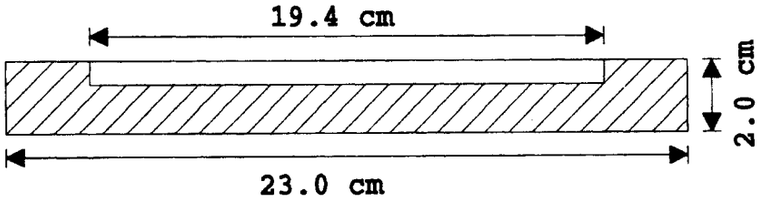

Cross Section View

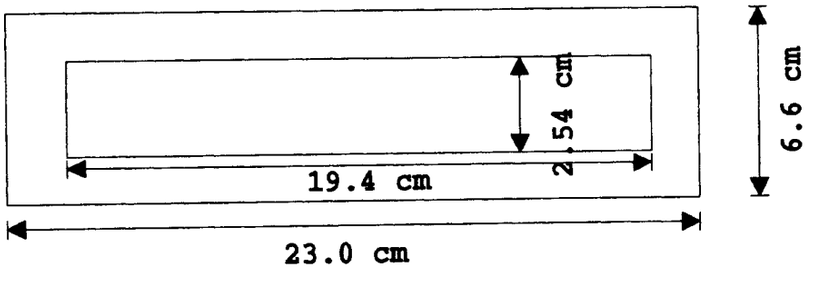

Top View

Figure 5. Aluminum Die

The data logging system included an analog interface card and software. An in-line torque meter was installed in the Meissner Rheometer to measure the amount of torque acting on the sample. For remote recording, a built-in potentiometer was installed in the torque monitor. The data logging system is for translating the voltage signal coming from the torque monitor into digital values. In our experiments, the digital value was translated to the torque acting on the sample so that the torque data could be read directly from the computer screen. Before running the experiment, the data logging system needed to be calibrated. The calibration procedure is listed in APPENDIX D.

During the experiment, the polymer sample was stretched to the desired Hencky strain at a constant extensional rate. Before running the computer controlled motor, the program using X-language (APPENDIX C contains a tutorial on how to use the X-language) needed to be developed to control the motor. To make certain the motor stopped after the polymer sample was stretched to the desired Hencky Strain (extensional rate times time) was very important. In X-Ware language, the distance command is in the form of "Dn". "D" specifies the distance and "n" means the motor will move n steps. Therefore, "n" defines the Hencky strain. If "n" is the same, even at different roller rotating speed, the sample will given same Hencky strain. For example, at a rotating speed of 0.1 RPM (extension rate 0.24 s^{-1}), "D7500" means the motor running time is 3 seconds and the Hencky

stain is 0.72. However, at a rotating speed of 0.05 RPM (extension rate 0.12 s^{-1}), "D7500" means the motor running time is 6 seconds and the sample has the same Hencky strain at 0.72. Therefore, fixing the "Dn" at different rotating speeds, the motor will stop at the desired Hencky strain.

In order to place the sample between the rollers, hydraulic jacks were used to elevate the rollers above surface of the oil, and the roller gap adjustment knob was turned to open a gap between the rotary clamps so that the polymer sample could be slid into place. Then the gap was closed to hold the sample securely. Releasing the jacks allowed the rollers and sample to be immersed in the oil. When the sample was immersed in the oil, the camera was adjusted to focus on the polymer sample.

When the position of the light source and the other elements on the optical train were set correctly, the heater was turned on and the temperature was set 5 °C higher (130 °C in the case of HDPE) than the melting point of the sample and held for 30 minutes to allow for equilibration and full melting. When the sample softened in the hot oil, the roller gap was readjusted to secure the sample in the roller teeth. The sample sagged because of thermal expansion. The rollers were rotated at very low rates to take out the slack in the polymer sample. At this time, the polarizer was rotated 45° counter clockwise and the analyzer was set perpendicular to the polarizer. If after 30 minutes, no birefringence was observed, the sample was assumed to be

completely molten. Then the temperature was set to the desired run temperature. The sample was held for at least 30 minutes at the run temperature to allow for complete thermal equilibration before applying the stress field.

Before starting the motor, checking that the torque monitor was at the zero position on the dial was very important.

The computer motor was controlled by the "RUN" program in the "WARE" sub-directory. The program was executed by typing "run" followed by a carriage return. "Terminal Emulator" was selected from the menu. In the terminal emulator, a series of commands like the following could be entered:

```
> H-
> Vn
> Dn
> Tn
> G
```

This series of commands resulted in a steady counter-clockwise motor rotation. In these commands, "H-" means the rollers are set to rotate in the direction as shown in Figure 6 to elongate the polymer sample. The rotation speed is in the form of "Vn" where "n" is the rotation speed in RPM. "Dn" defines the running time, after distance "n", the motor will stop. At exactly the same time as the return key was hit, the VCR was set to record (the beginning time of

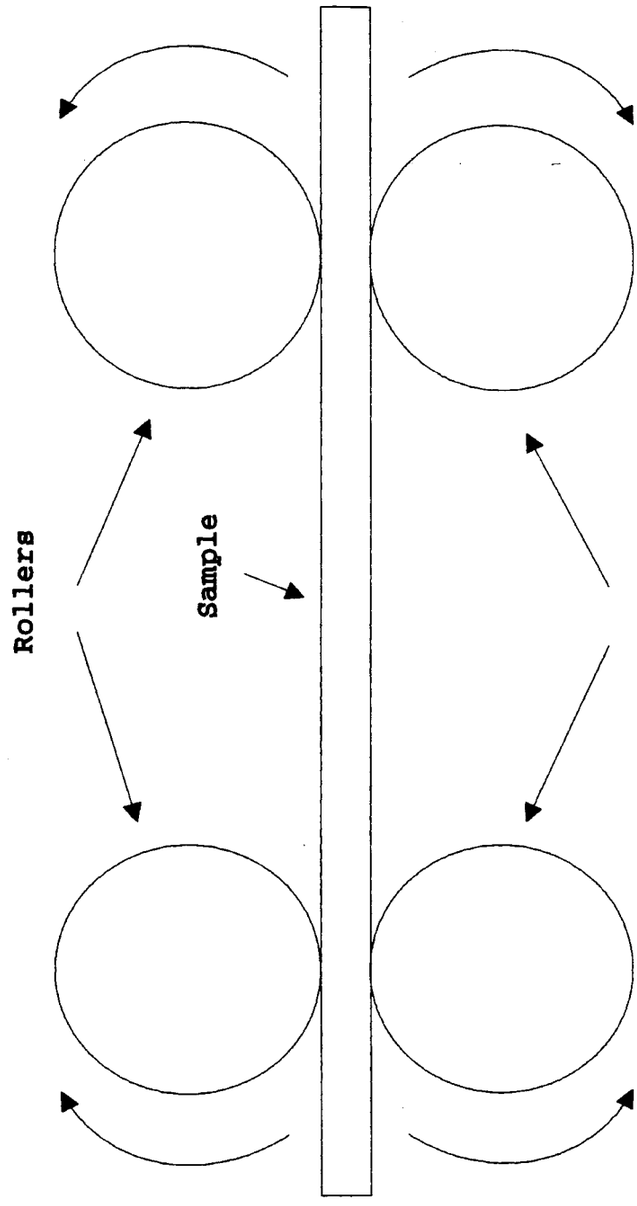

Figure 6. Flow Direction

the videotape was recorded so that the beginning time of stretching the sample could be determined when the videotape was replayed) and the stopwatch was also set to start.

The reason the motor was set to run after "n" seconds is that time was required to enter into the data logging software before the experiment began. The data logging software stored the torque data while the experiment was running. To enter into the data logging software, "LOG_SRCA" was typed to run the program, "Gather Data" was selected from the main menu and then the data file name was defined. The software recorded three torque data points every second during the experiment. When starting to record the torque data, the stopwatch was stopped so that the beginning time of stretching could be identified in the data file. The motor would stop after a desired Hencky strain. The VCR was kept recording for 60 minutes or more and the birefringence pattern and torque data could be analyzed later.

Data Analysis

The stress acting on the sample could be calculated from the equation:

$$\tau_{zz} - \tau_{xx} = \frac{T_r}{rA} \qquad (6)$$

where:

$\tau_{zz} - \tau_{xx}$ = first normal stress difference

T_r = torque acting on the sample

r = radius of the roller

A = cross sectional area of the sample.

The thickness of the sample could be calculated from:

$$d = \frac{d_0 w_0}{\exp(\varepsilon t) w} \tag{7}$$

where

d = thickness of the sample

d_0 = initial thickness

w_0 = initial width

w = width at any time

t = time

ϵ = strain rate.

In order to quantify the flow-induced kinetics, the retardation of the crystallizing system was needed. As discussed in Chapter II, the total retardation of our system, δ_{tot}, is equal to

$$\delta_{tot} = \delta_a + \delta_{da} + \delta_c \tag{8}$$

where:

δ_a = retardation of the amorphous carrier phase (in our experiment, δ_a equals to zero because the silicon oil which was the carrier phase has no retardance)

δ_d = retardation of the amorphous sample phase

δ_c = retardation of the crystalline regions of the

sample.

The retardation in the sample can be obtained by simplifying Equation (4):

$$T = \frac{1}{4}\sin^2\left(\frac{\pi L\Delta}{\lambda}\right)[1 - \cos 4(\chi - \alpha)] \qquad (9)$$

In our experiment, the reference direction was taken as χ = 0 and the angle $\alpha = 45^{\circ}$. So Equation (4) was simplified to:

$$T = \frac{1}{2}\sin^2\left(\frac{\pi L\Delta}{\lambda}\right). \qquad (10)$$

Combined with Equation (3), Equation (10) could be expressed by:

$$T = \frac{1}{2}\sin^2(\pi R). \qquad (11)$$

Since the retardance $\delta = 2\pi R$, Equation (11) becomes:

$$T = \frac{1}{2}\sin^2\left(\frac{\delta_T}{2}\right) \qquad (12)$$

By definition, the fraction of transmitted light T is equal to I/I_0. Equation (12) could be inverted to obtain the total retardance:

$$\delta_{tot} = 2\sin^{-1}\left[\left(\frac{2I}{I_0}\right)^{\frac{1}{2}}\right] \qquad (13)$$

where

δ_{tot} = total test section retardance

I = the intensity of the transmitted light

I_0 = the intensity of the incident light beam.

In order to obtain the retardance, δ, a video image technique was used. The pixel value at each point of the flow field was obtained by running the computer software. By typing "IR" to run the program in the "IRIS-t" sub-directly. By replaying the videotape frame by frame and placing the cursor at different points on the video image on the screen pixel value can be obtained. Normally, 9 points were selected from the video image and the average pixel value was calculated.

However, the pixel value is not the same as the intensity of light which is needed for analysis. In signal transmission, there is a function called a "look up table" which assigns a pixel value to an absolute intensity of transmitted light. Each experimental run had a different look up table. The following procedure was used to convert pixel values to intensity of light and fraction of transmitted light for each experimental run.

1. The pixel value was plotted as a function of time and the peak value was identified.

2. Fraction of transmitted light T, by Equation (12), has a value of 0.5 at the peak pixel value.

3. Use Equation (12) to obtain the fraction of transmitted light at any point for which the pixel value was

known.

4. The values of T at any point could be found by linear interpolation between two points at which the gray value and the value of T were known.

5. Intensity of transmitted light could be obtained by multiplying the T value with the peak value of transmitted light.

Total retardance could be found by inversion of Equation (12):

$$\delta_{tot} = 2N\pi \pm 2\sin^{-1}[(2T)^{\frac{1}{2}}] \qquad \textbf{(14)}$$

Where N is equal to 0, 1, 2, 3,.....N.

Summary

In the experimental work, the modified Meissner Rheometer was used and a new experimental technique was developed.

The data logging system was used to allow easy and precise torque data acquisition. A new method was developed to produce smooth and homogeneous polymer samples. A new experimental technique and procedure were also developed to obtain the flow-induced crystallization kinetic data.

CHAPTER IV

RESULTS AND DISCUSSION

In the experiment, the birefringence of a molten high density polyethylene sample undergoing extensional flow was observed. The birefringence behavior was converted to kinetic data which agreed with the data of other investigators. The results have been obtained over a wider range of extensional rate, and with less effort than those reported previously.

Raw Data

Figure 7 shows the typical development of birefringence with time in a HDPE sample at 125 °C, an extension rate of 0.24 s^{-1} and a strain of 0.72. The photograph in Figure 7a was taken before the stress was applied to the sample. The two bright areas are the light coming through the upper and lower part of the circular optical window. The polymer strip obstructs the light from the middle of the window so that the middle section is completely dark, indicating that the sample was totally molten, completely amorphous and the molecules were randomly oriented. The sample was then stretched. Figure 7b shows the birefringence pattern 2

7a. Before stress

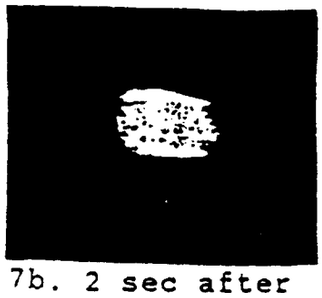

7b. 2 sec after onset of flow

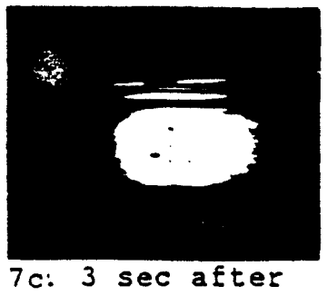

7c. 3 sec after onset of flow (flow ceased)

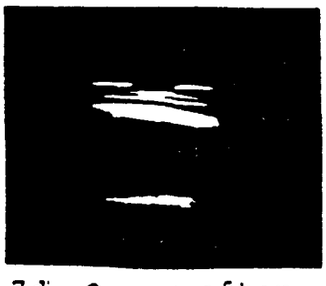

7d. 2 sec after cessation

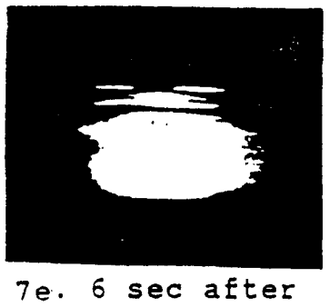

7e. 6 sec after cessation

7f. 18 sec after cessation

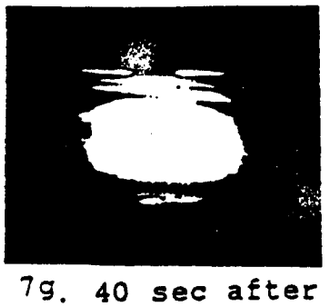

7g. 40 sec after cessation

7h. 79 sec after cessation

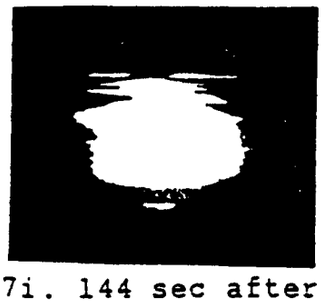

7i. 144 sec after cessation

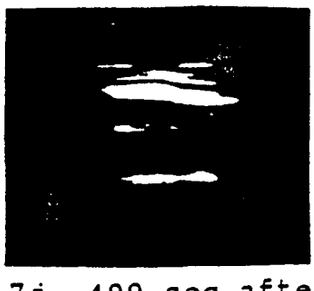

7j. 499 sec after cessation

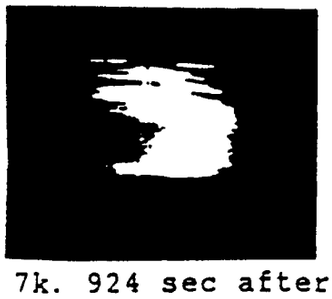

7k. 924 sec after cessation

Figure 7. Birefringence Behavior at Temperature of 125 °C, Extensional Rate of 0.24 s^{-1}, Extensional Strain of 0.72.

seconds after the onset of flow. The partially transmitted light in Figure 7b indicates that the molecules had started to orient along the horizontal axes. Figure 7c shows the birefringence pattern at the time of flow cessation (3 seconds after the onset of flow). Figure 7d shows that the fraction of transmitted light decreased right after the cessation of flow. McHugh, Guy and Tree (14) reported similar behavior which was attributed to the relaxation of the amorphous phase. After the intensity had decreased to a minimum value, shown in Figure 7d, the light intensity increased until a peak value was reached which is shown in Figure 7e. The fraction of transmitted light went through cycles of increase and decrease over the next 60 minutes until a near constant value was reached (Figure 7k). Maximum values of light transmission were reached at 40 seconds and 144 seconds after cessation of flow; Figures 7g and 7i respectively. Minimum values of light transmission were observed at 18 seconds, 79 seconds and 499 seconds after cessation of flow; Figures 7f, 7h and 7j respectively. The repeated increase and decrease of light transmission in a molten polymer system undergoing extensional flow has not been previously reported.

Pixel Value and Torque as Function of Time

The images shown in Figure 7 were converted to quantitative pixel values by using the computer software and techniques described in Chapter III. Figure 8 and 9 show

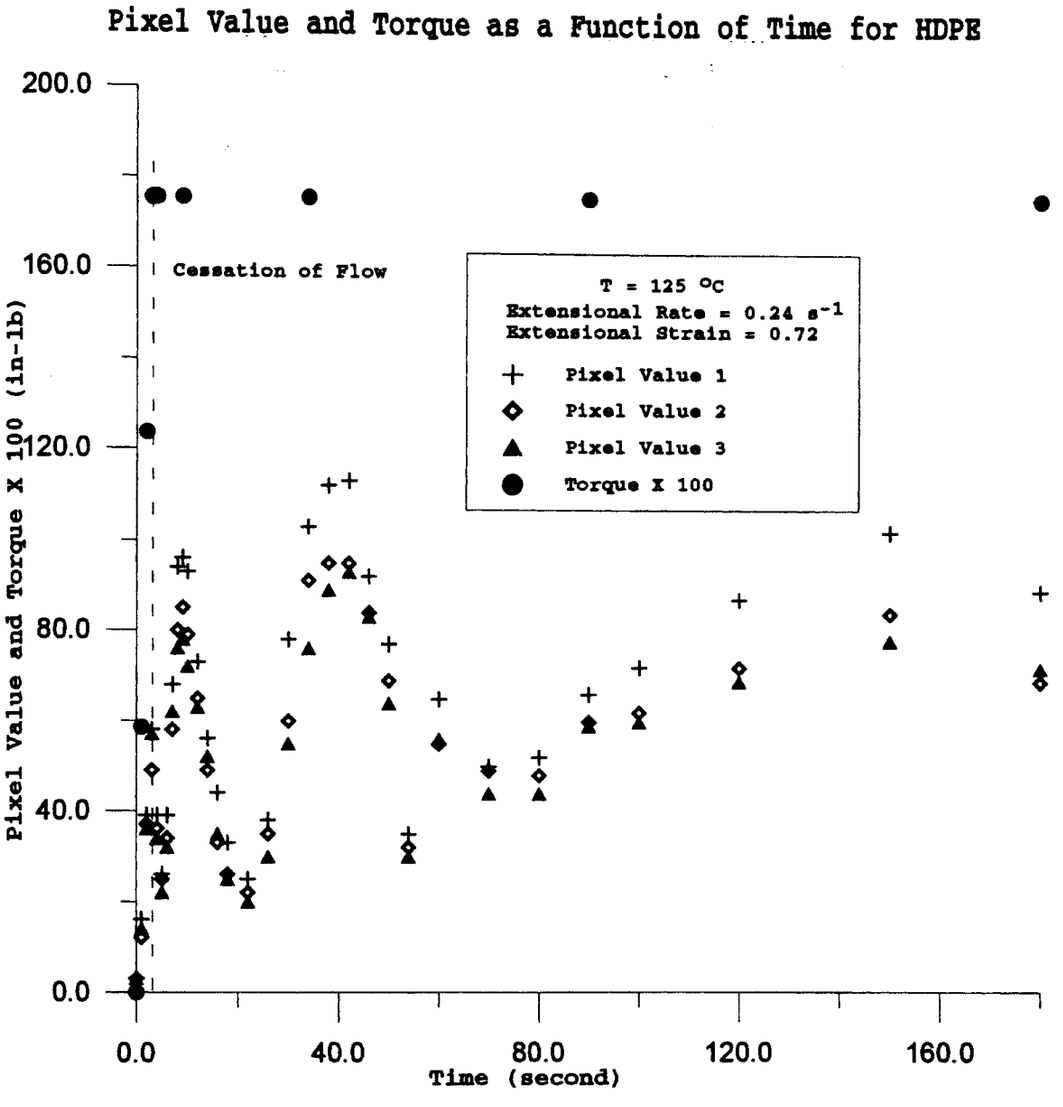

Figure 8. Pixel Value and Torque as a Function of Time

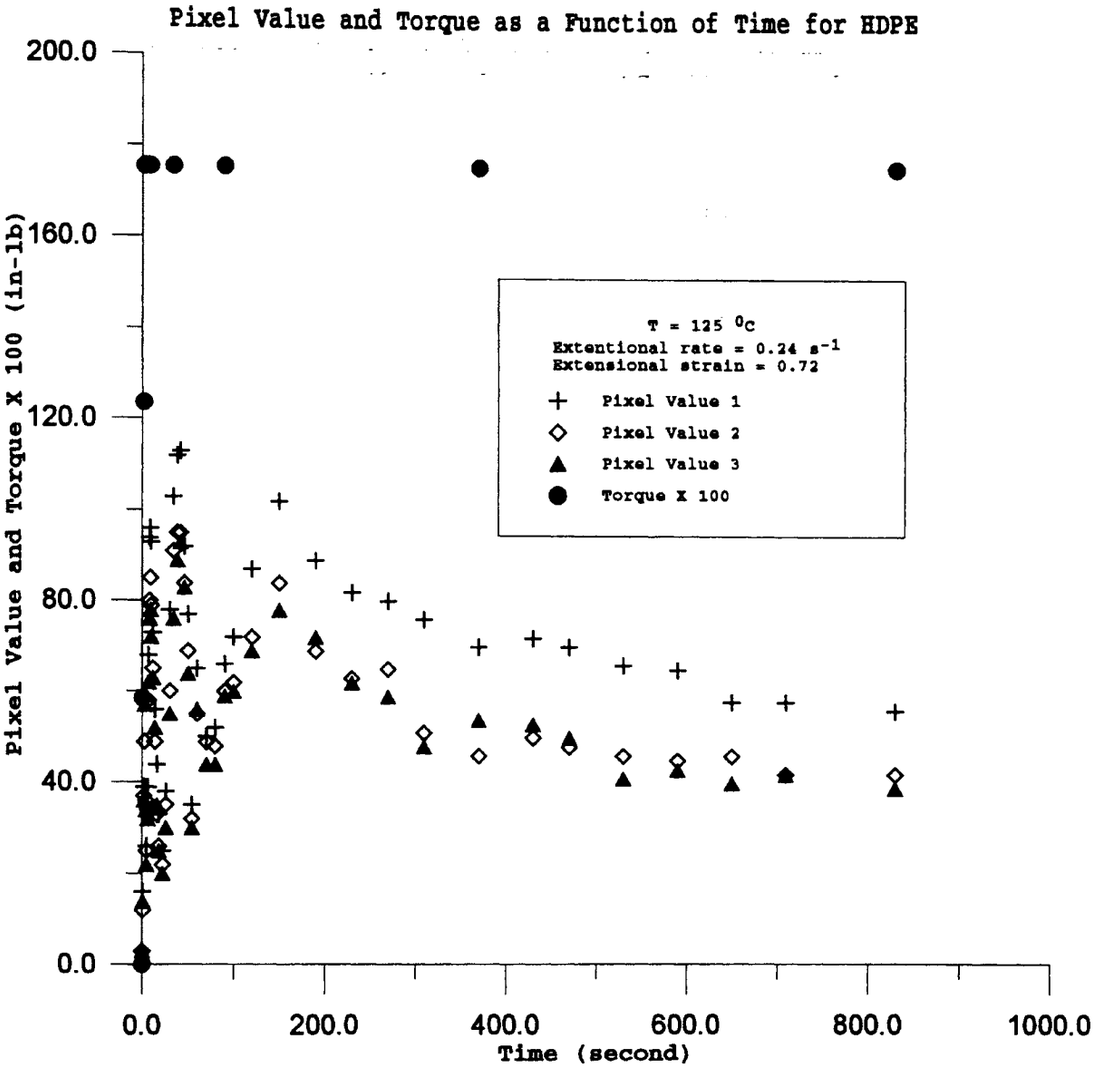

Figure 9. Pixel Value and Torque as a Function of Time

the pixel values and torque data for the same experiment as was shown in Figure 7. Figure 8 and 9 were plotted on different time scales to emphasis the beginning of the run (Figure 8) and the end of the run (Figure 9). In each of the figures, three different points on the sample were selected for analysis.

The point at time equals zero (in Figures 8 and 9) corresponds to Figure 7a at the very beginning of the experiment. As expected, both the torque and pixel value are zero. At the beginning of the experiment, the fraction of transmitted light increases as the torque increased and reached a local maximum at the same time as the cessation of deformation. After the deformation ended, the torque value remained constant, while the pixel value decreased. As discussed in the previous section, the decrease in pixel value was attributed to amorphous orientation. However, soon after the cessation of deformation, the pixel value began to rise until a maximum was reached at 6 seconds after cessation of flow corresponding to Figure 7e. Figure 8 and 9 clearly show cycles of increasing and decreasing pixel intensity as would be expected from the photographs in Figure 7. Figure 9 shows that the pixel value eventually reached a near constant value at long times.

Intensity of Transmitted Light and Fraction of Transmitted Light

As discussed in Chapter III, the pixel value is not the

same as the intensity of light which is needed for analysis. Therefore, the pixel values were converted to the absolute intensity of transmitted light using the technique described in Chapter III.

In Figure 10, intensity of transmitted light and fraction of transmitted light value were plotted as a function of time for the same experimental run shown in Figures 7 to 9. Other intensity data are listed in Appendix E. The intensity value shown in Figure 10 had exactly the same trend as the pixel value shown in Figure 8 with a little difference in the value. The intensity value shown in Figure 10 reflected the absolute intensity of transmitted light that was seen on the screen and Figure 7. The fraction of transmitted light shown in Figure 10 reflected the transmittance which was the ratio of intensity of transmitted light to twice the peak value of intensity of transmitted light. With the same trend as the pixel value shown in Figure 8 and Figure 10, the increasing intensity of light after onset of the flow indicated that the polymer molecules started to orient under the applied stress. Two seconds after cessation of flow, the intensity of light decreased to minimum value because of the relaxation of the amorphous phase. The intensity did not decrease to zero because during the flow period, a small amount of crystal formed in the sample and caused the birefringence. Then, the intensity increased and reached peak value at 6 seconds after cessation of flow shown in Figure 10. After the

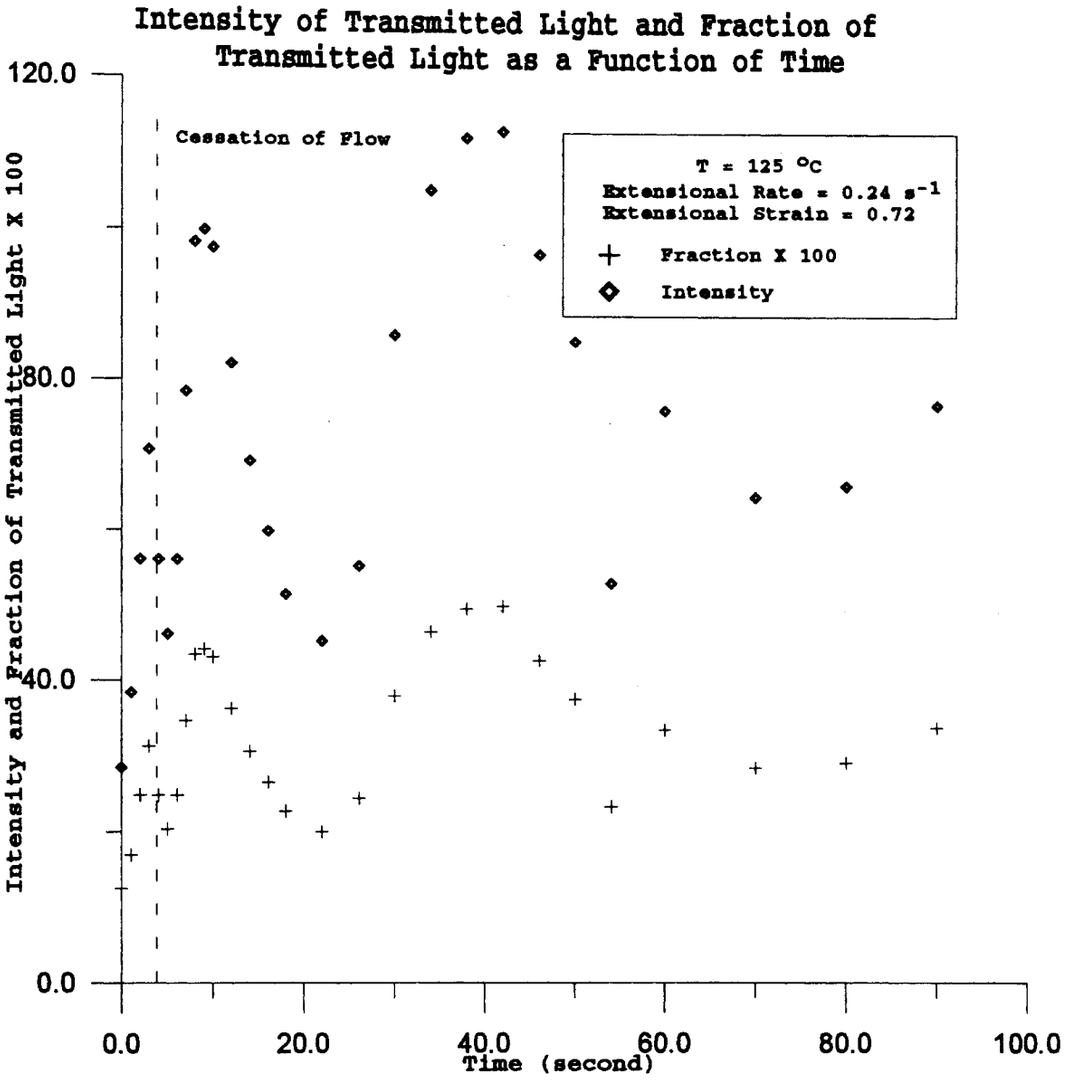

Figure 10. Intensity of Transmitted Light and Fraction of Transmitted Light as a Function of Time

intensity decreased to minimum value, it increased again. The cycle of increase and decrease repeated four times in next 60 minutes. We believe that the increase and decrease behavior indicated the development of extended chain crystals after the cessation of flow as is discussed later in this chapter.

Retardance

The intensity of transmitted light shown in Figure 10 was converted to retardance, which is directly related to flow-induced crystallization, and shown in Figure 11. The other plots of retardance as a function of time are listed in Appendix E. The inversion of the light transmission equation to obtain the retardance and detailed analysis technique and procedure were described in Chapter III. Figure 11 shows a increasing value of retardance after the cessation of flow indicating the development of crystallization. This result is in agreement with the data presented by Tree (1) and Guy (14).

Reproducibility

Two experiments were run at the same temperature of 125 °C, an extension rate of 0.24 s^{-1} and a strain of 0.72. The results were plotted together as function of time in Figure 12. The pixel values and torque data have the same trend that pixel value has cycles of increase and decrease while the torque remains the same after the cessation of

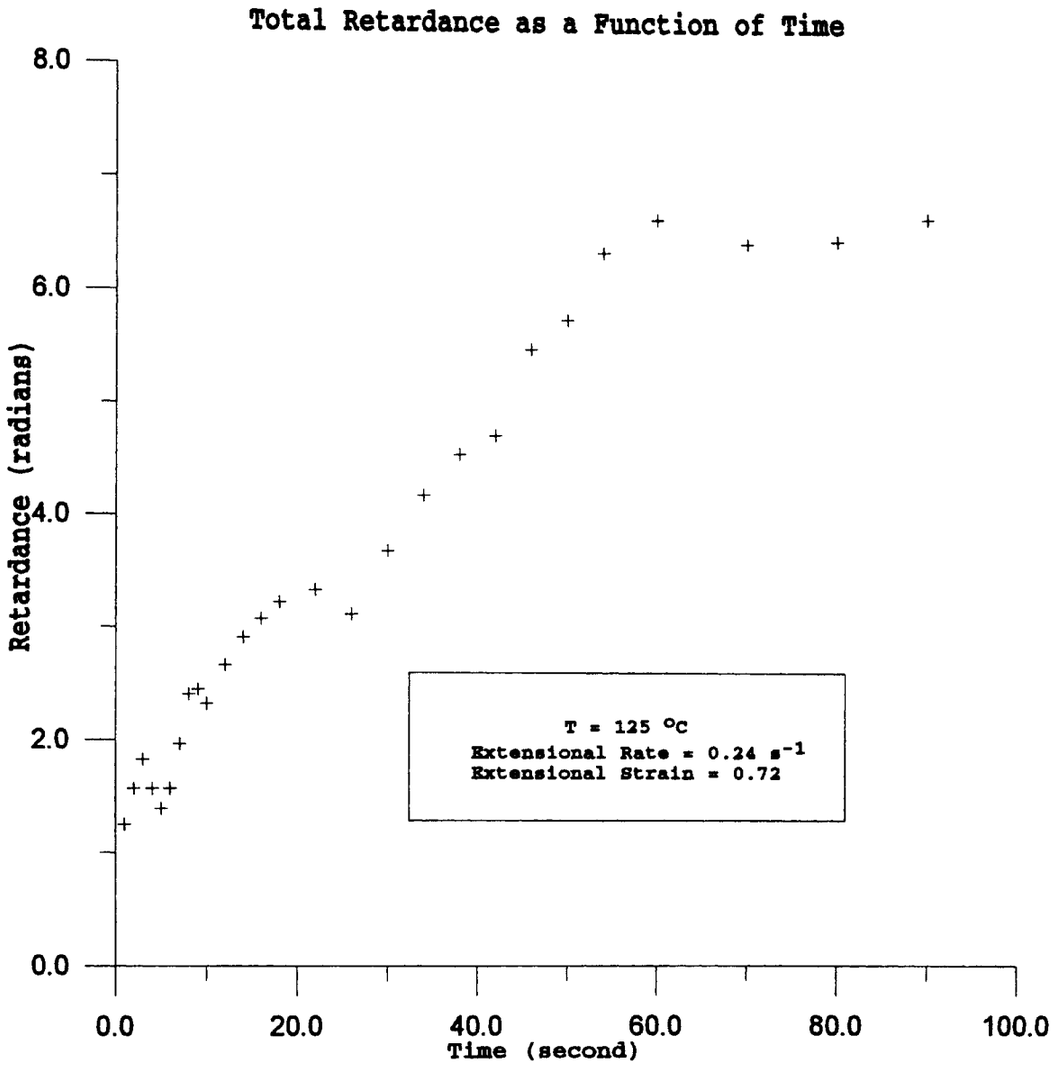

Figure 11. Retardance as a Function of Time

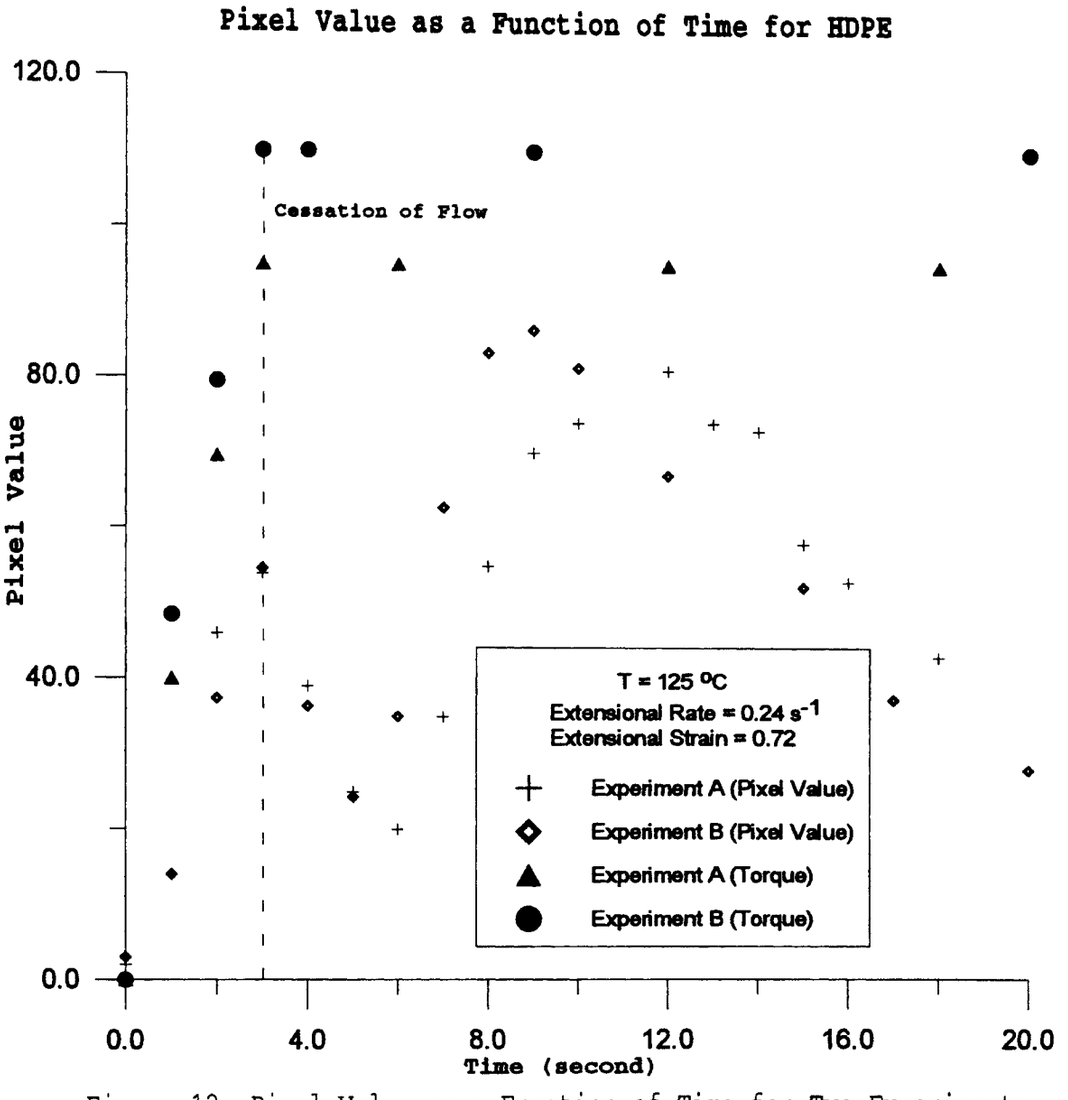

Figure 12. Pixel Value as a Function of Time for Two Experiments

flow. However, a difference still exists between the two sets of data. The error may have come from limitations of the experiment such as: sample preparation, temperature control or imperfections in the rheometer clamps (irregularity of teeth and difference in distance of gaps between two adjacent rollers).

Comparison to Previous Results

As discussed in Chapter II, the measurements of extensional flow-induced crystallization kinetics have been non-existent except for those of Tree (1) and Guy (14). One of Guy's experimental data at temperature of 135.6 °C and an extension rate of 0.031 s^{-1} is shown in Figure 13. The generalized transmitted light intensity behavior (as a function of time) for a typical flow-cessation experiment was presented by Guy (14) in Figure 14. The results of our experiment shown in Figure 15 was for a run at 125 °C, extensional rate of 0.03 s^{-1} and extensional strain of 0.60. In Figure 15, the intensity of transmitted light decreased rapidly after the cessation of flow due to relaxation of the amorphous phase, then increased to a maximum value due to crystallization and decreased afterwards. Guy's data shown in Figure 13 has the same intensity behavior at this low extensional rate (0.03 s^{-1}). The repeated increase and decrease behavior of intensity of light we observed at high extensional rates (0.24 s^{-1}) has never been reported.

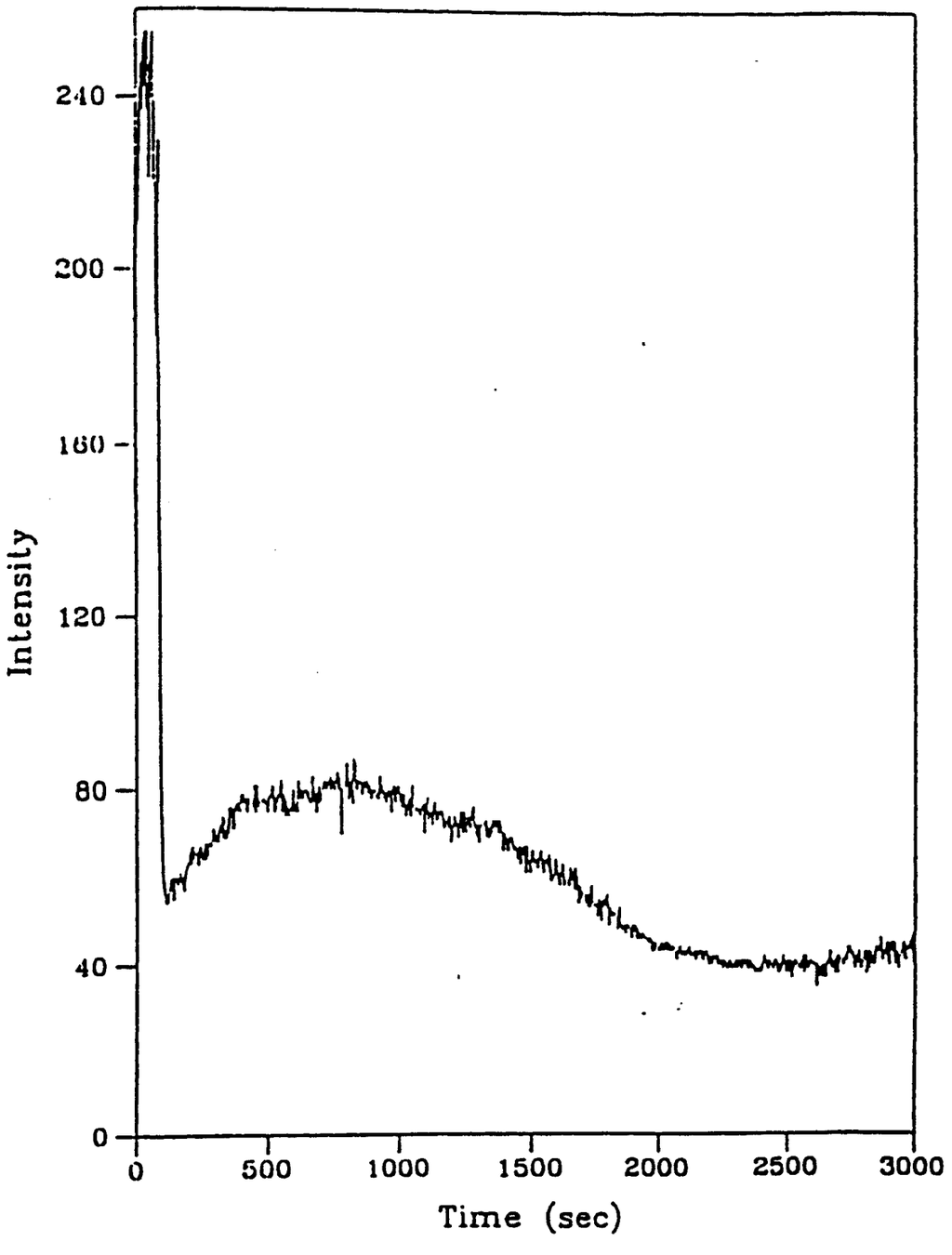

Figure 13. Intensity as a Function of Time at
Temperature = 135.6 ^{0}C
Extensional rate = 0.032 s^{-1}
(14)

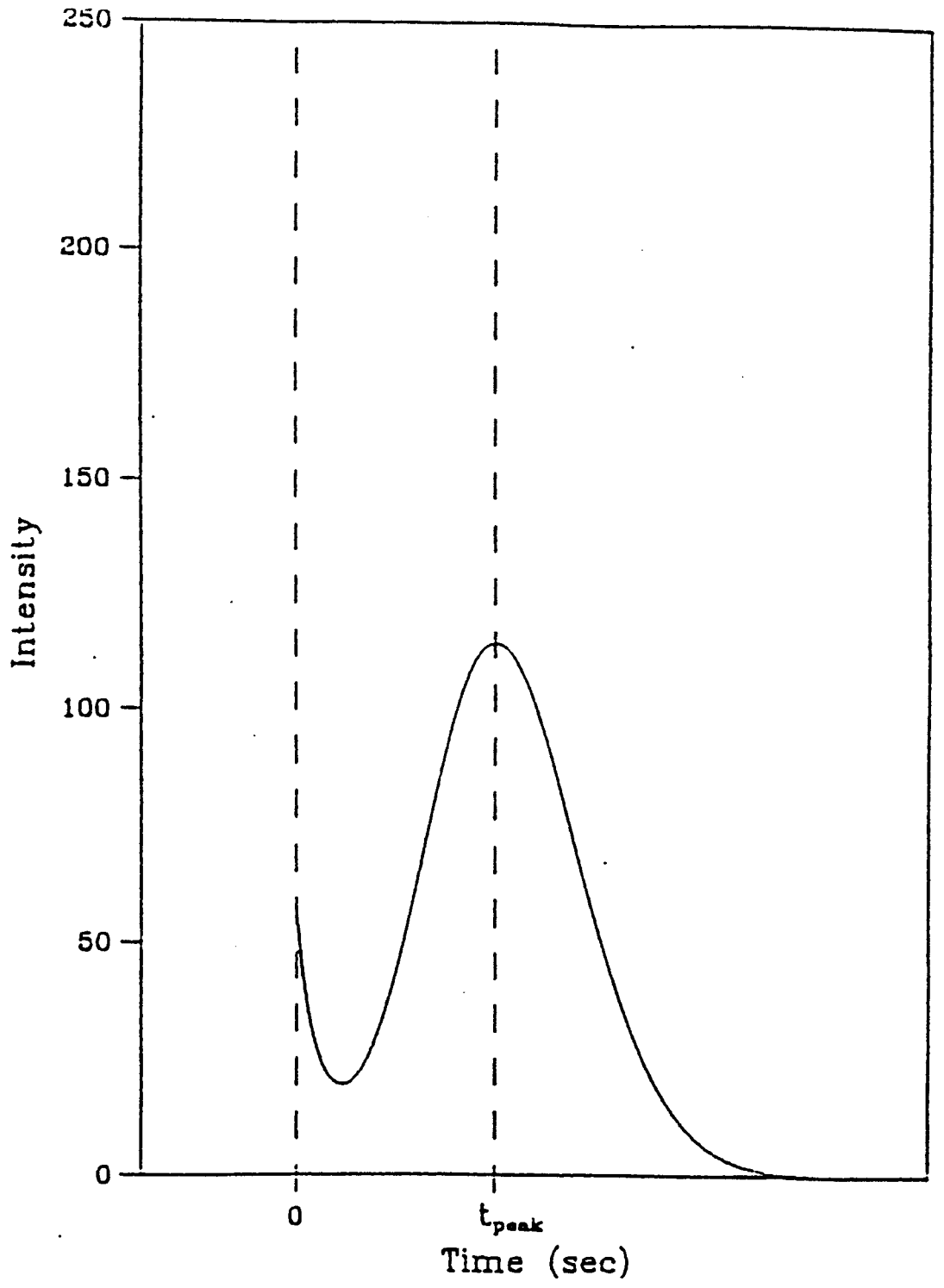

Figure 14. Generalized Light Intensity Behavior After Cessation of Flow (14)

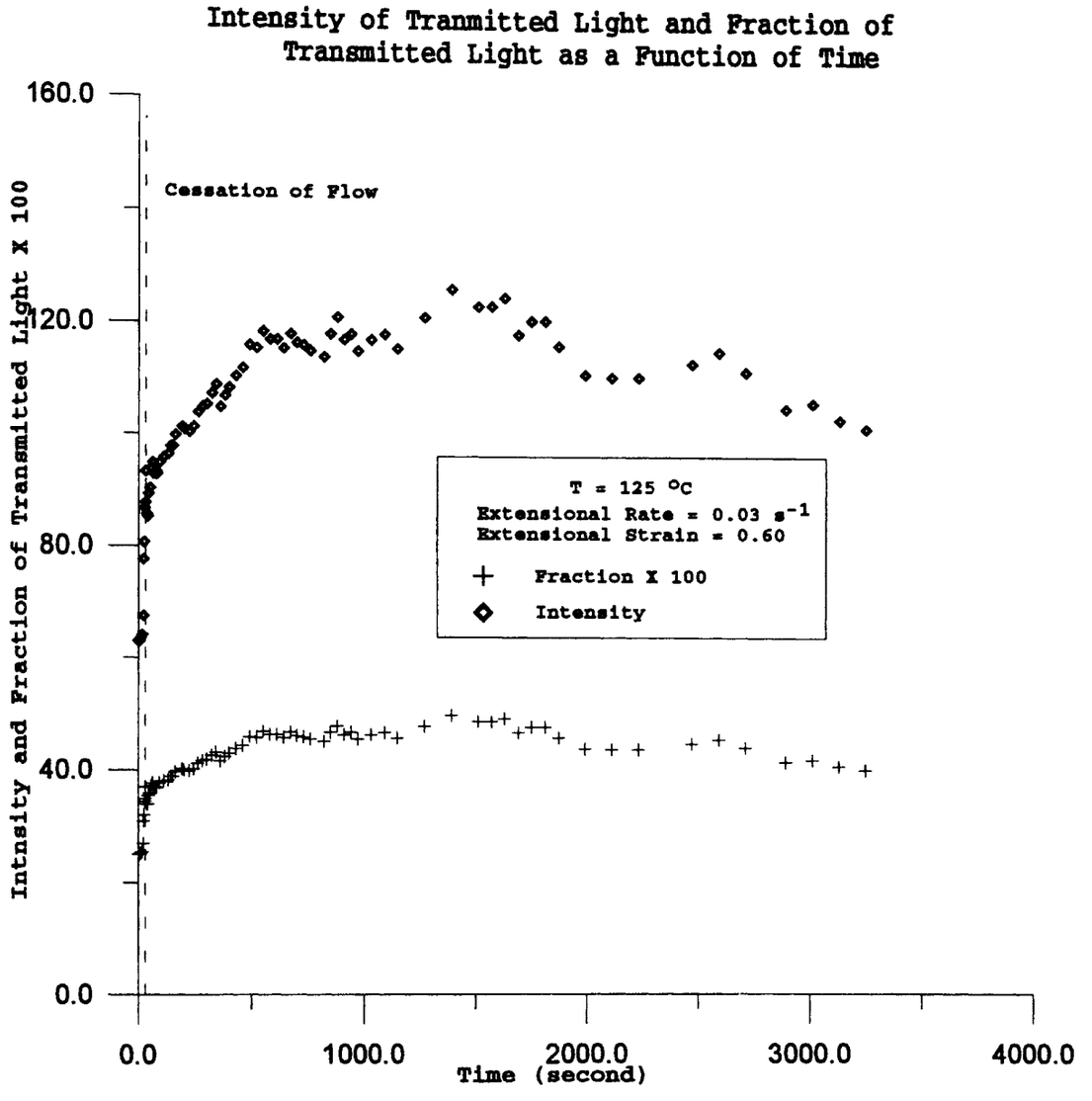

Figure 15. Intensity of Transmitted Light and Fraction of Transmitted Light as a Function of Time

Advantage of the Experiment

Guy's experimental results were limited to very low extensional rate (< 0.032 s^{-1}) because of the two-phase blend flow. In our experiment, the birefringence data, shown in Figure 8 and Figure 16, were obtained over a wider range of extension rate from 0.03 s^{-1} to 0.24 s^{-1}.

Properly inserting the crystallizable droplet phase into the LLDPE carrier phase and the two-phase flow characterization made Guy's experimental work very difficult. However, in our experiment, obtained the data was simply done by clamping the polymer sample between two pairs of rotary clamps, submerging into the silicon oil, running the computer controlled motor, recording and analyzing the birefringence behavior.

Discussion

Generalized intensity of transmitted light as function of time upon cessation of flow of our experiment, which represented the experiment run at the extensional rate of 0.24 s^{-1}, is shown in Figure 17. After cessation of flow, the torque remained at the same value while the intensity of transmitted light increased indicating the growth of crystals in the sample. Because increasing intensity of transmitted light includes two parts: increasing of intensity due to crystallization and increasing of intensity due to orientation. The only way to increasing the

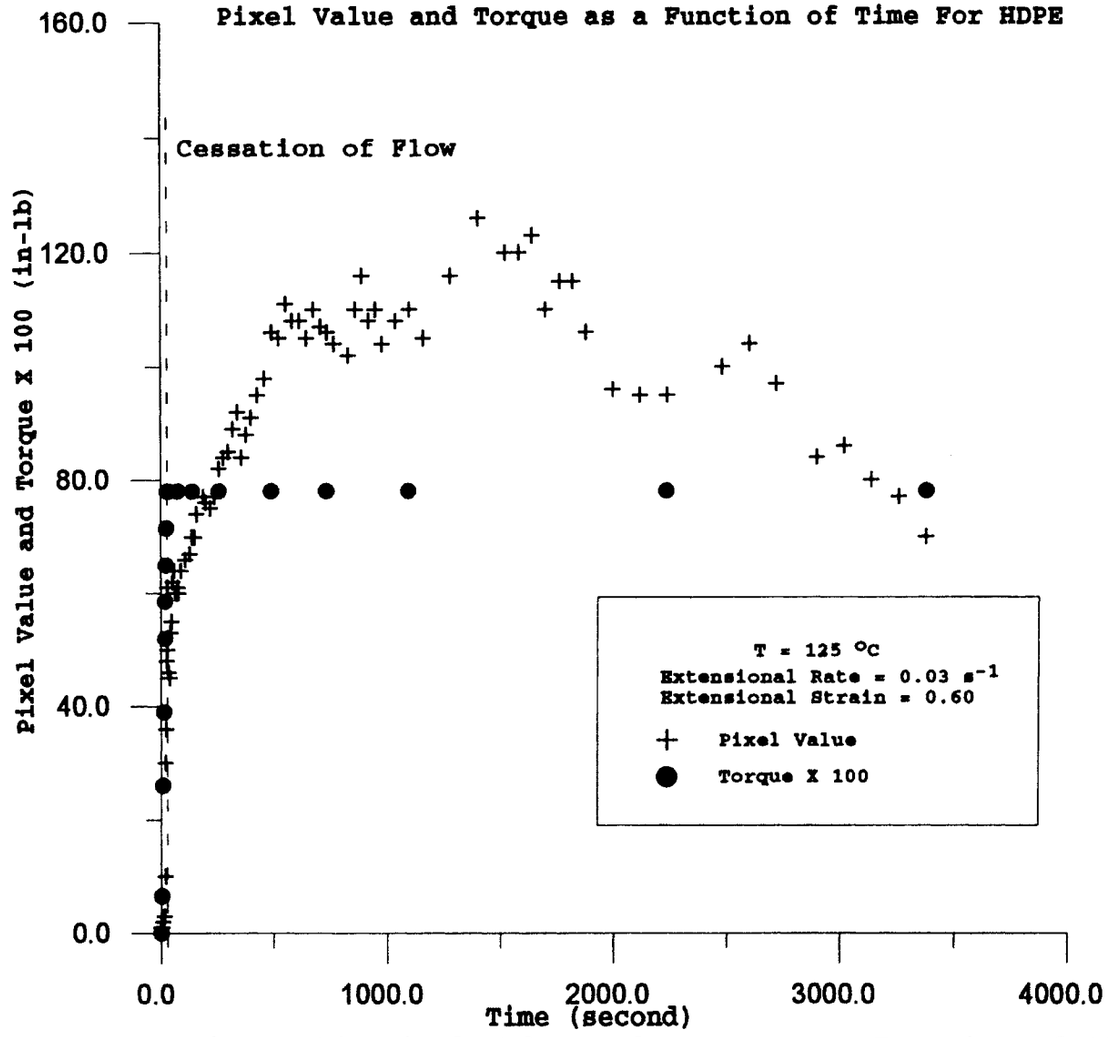

Figure 16. Pixel Value and Torque as a Function of Time

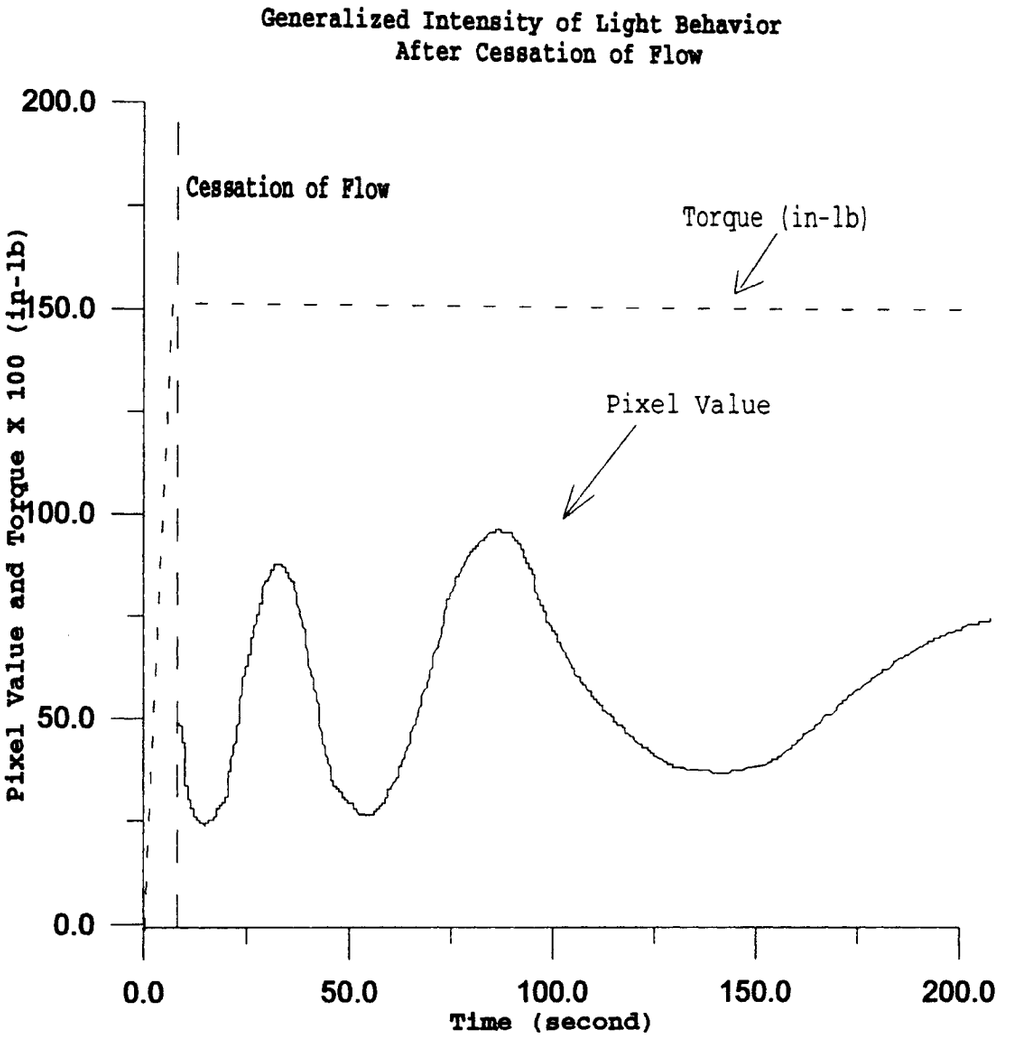

Figure 17. Generalized Light Intensity Behavior
After cessation of Flow

orientation is to apply the stress (1). From the results, the stress remain the same after the cessation of flow, so the increase in intensity means the crystals formed after the cessation of flow.

In Figure 15, the intensity first reached its peak value after cessation of flow, and then decreased as we described above. After that, the intensity increased and decreased four times in the next 60 minutes. One possible explanation about this kind of behavior is that from equation (12) the transmitted intensity of light was changing with a Sin function. When more and more crystals formed in the sample, the retardance kept increasing, and the term $\sin(\delta_{tot})$ changed. Thus the intensity of light goes "up and down" with time.

Limitation of the Instrument

Following limitations of the instrument should be noticed:

1. The flow field generated by the modified Meissner rheometer was assumed to be pure extensional flow along the horizontal axis of the sample. The difference in the gap space between two pairs of adjacent rollers, irregular teeth on the surface of rollers and end effects caused by clamped the sample at two ends may cause nonuniform extensional flow.

2. The sample made from the technique described in Chapter II was assumed to be homogeneous. All the samples

used in the experiments were considered exactly the same. Actually, it is impossible to make a totally homogeneous sample, and any difference in the process of producing the sample may cause some differences between samples.

3. The temperature was assumed uniform in the oil bath and the sample while the heat loss from the wall of the oil bath may lead to a temperature gradient between the sample and the wall.

CHAPTER V

SUMMARY, CONCLUSION AND RECOMMENDATION

Summary

The primary goal of the experimental work was understanding the flow-induced crystallization kinetics of polyethylene in an extensional flow field via analysis of birefringence and torque data.

The extension flow was generated by a modified Meissner Rheometer with two pairs of rotating clamps. The homogeneous deformation along the horizontal axis of polyethylene sample was produced by stretching the ends of the sample. The birefringence behavior was recorded and analyzed using video imaging and digitizing techniques. Torque data was recorded by a data logging system.

Conclusions

1. The modified Meissner Rheometer used in the experiment proved that a nearly homogeneous extensional flow could be generated and that the equipment setup overcame many of the experimental difficulties in the study of flow-induced crystallization in extensional flow.

2. An experimental technique and procedure were developed to record the birefringence behavior and torque acting on the polymer sample during the flow-cessation experiment and to convert the birefringence images to quantify data using video image analysis.

3. The results were qualitatively consistent with the data that Guy (14) had presented. Our data were reproducible and could be obtained over a wider range of conditions with less effort.

Recommendations

1. The Modified Meissner Rheometer is suitable for use in the further study of flow-induced crystallization.

2. The stainless steel shafts in the rheometer should be thicker to prevent bending when the sample is clamped.

3. The tooth pattern of four rollers should be made more uniform so that the irregularity of the tooth could be eliminated and the sample could be given a more uniform deformation.

4. A computer program should be developed to read the pixel values from the video image in any position of the sample and in any desired time interval.

5. Dichroism is recommended to be monitored to give a more direct indicator of the presence of crystal since birefringence is sensitive enough only to low levels of crystallinity.

6. Other crystallizable polymers such as polypropylene

should be examined to help further study of flow-induced crystallization in extensional flow and a non-crystallying system such as polystyrene should be examined for comparison of stress and birefringence behavior.

BIBLIOGRAPHY

(1) Tree, D. A., "Crystallization Kinetics of Polymer Melts in Extensional Flow", Ph.D. Thesis (Chemical Engineering), University of Illinois, Urbana, Illinois (1990).

(2) Van der Vegt, A. K. and Smit, P. P. A., S. C. I. Monograph, 26, 313 (1967).

(3) Seigloff, C. I. and O'leary, K. J., J. Macromol. Sci. Phy., B2(4), 793 (1968).

(4) Seigloff, C. I. and O'leary, K. J., Trans. Soc. Rheol., 14:1, 49 (1970).

(5) Southern, J. H. and Porter R. S., J. Appl. Polym. Sci., 14, 2305 (1970).

(6) Southern, J. H. and Porter R. S., J. Polym. Sci., A-2, 10, 1135 (1972).

(7) McHugh, A. J., Tree, D. A., Pornnimit, B., Ehrenstein, G. W., Int. Polym. Process., 6, 208 (1991).

(8) Tsebrenko, M. V., Reganova N. M. and Vinogradov G. V., Polym. Eng. Sci., 20, 1023 (1980).

(9) McHugh, A. J. and Tree, D. A. Int. Polym. Process., II:3/4, 223 (1988).

(10) Tree, D. A., M.S. Thesis (Chemical Engineering), University of Illinois, Urbana, Illinois (1987).

(11) Titomanlio, G. and Marrucci, G., AICHE J. 36, 13 (1990).

(12) Ness, J. N. and Liang, J. Z., J. Applied Polym. Sci., 48, 557 (1993).

(13) Sakellarides, S. L. and McHugh, A. J., Polym. Eng. Sci., 27(22), 1662 (1987).

(14) McHugh, A. J., Guy, R. K. and Tree, D. A., Coooid Polym. Sci., 271, 629 (1993).

(15) Vrahopoulou-Gilbert E. and McHugh, A. J., Macromolicules,17, 2657 (1984).

(16) Vrehopoulou E. P. and McHugh, A. J., J. Appl. Polym. Sci., 31, 399 (1986).

(17) Spevacek, J. A. and McHugh, A. J., J. Polym. Sci. Phy., 29, 969 (1991).

(18) Young, W. S. and McHugh, A. J., J. Polym. Sci., 270, 431 (1989).

(19) McHugh, A. J., Vrahopoulou, E. P. and Edwards, B. J., J. Polym. Sci. Phy., 25, 953 (1987).

(20) McHugh, A. J., Burghardt, W. R. and Holland, D. A., Polymer, 27, 1585 (1986).

(21) McHugh, A. J. and Rietveld, J., J. Polym. Sci., Phy. 23, 2359 (1985).

(22) Rietveld, J. and McHugh, A. J., J. Polym. Sci., Phy. 23, 2339 (1985).

(23) Siddiquee, M. S. Thesis (Chemical Engineering), Oklahoma State University, (1992).

(24) Elyashevich, G. K., Karpov E. A., Rosova E. YU. and Streltses B. V., Polym. Eng. and Sci., 33, 1341 (1993).

(25) Salem, D. R., Polymer, 33, 3182 (1992).

(26) Salem, D. R., Polymer, 33, 3189 (1992).

(27) Pazur, R. J. Ajji, A. and Prud'homme, R. E., Polymer, 34, 4009 (1993).

(28) Voice, A. M., Bower B. I. and Ward I. M., Polymer, 34, 1154 (1993).

(29) Voice, A. M., Bower B. I. and Ward I. M., Polymer, 34, 1164 (1993).

(30) Kaito, A., Nakayama, K. and Zubaidi, J. Appl. Polym. Sci., 45, 1203 (1992).

(31) Chang, C. L., Chiu, W. Y., Hsieh, K. H. and Ma, C.-C. M., J. Appl. Polym. Sci., 50, 855 (1993).

(32) Meissner, J., Raible, T. and Stephenson S. E., J. Rheology, 25, 1 (1981).

APPENDIX A

DATA LOGGING SYSTEM

Cole-Parmer's Data logging system was used to obtained the torque data that acted on the polymer sample during the experiment. The data logging system includes a Model #08109-32 Data Logging Software Package, a Model #08109-25 15-BIT A/D Card and a Model #08109-35MV/Amplifier/Multiplexer. Cole-Parmer's #08109-32 (PC64) data logging software is a flexible general purpose data acquisition package. The data are displayed on the screen and can be logged or charted on a printer. Data can be stored automatically at a preset interval and stored on disk or printed at rates from one scan/day to one scan/0.3 second. In the experiment, data were stored at the rate of one scan/0.3 second. Up to 64 channels of analog input can be accommodated; each with its own label, scaling factors and high and low limits. Up to 4 external multiplexers or thermometers can be used. The software was written in BASIC and recompilable by Microsoft QuickBASIC. Control functions or custom features can be added. The menu drive of the data logging software is shown in Figure A-1.

Cole-Parmer's #08109-25 (Model 14C) Analog Interface card enables an IBM PC to translate continuously variable analog voltages into their digital equivalents of ones and zeros. There are four address that can be changed by altering the switch settings on the Analog Interface. The card used in the experiment has four small switches in the upper left corner. Make certain that switch "4" is in the "on" position and the other three switches are in the "OFF"

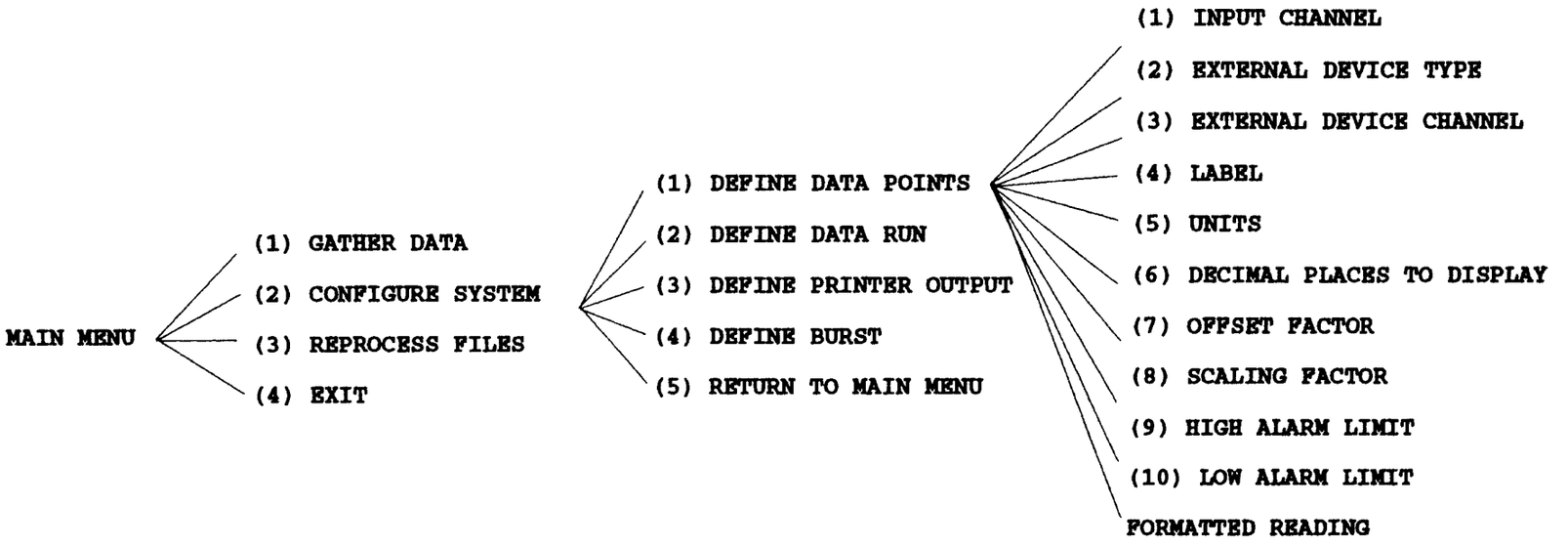

Figure A-1. Menu Drive of Data Logging Software

position. The switch set maps the Analog Interface into input location 772 in the experiment. When install the card, attach wires to a mating 15-pin connector. The connector pinout is shown is Table A-1.

Cole-Parmer's #08109-35 (Model 20A) Mv/Amplifier/Multiplexer in combination with the Model #08109-25 (Model 14 PC) A/D card allows a personal computer to be used as a multichannel milivoltmeter and amplifier. The interconnection diagram between the Model #08109-35 and the A/D card is shown in Figure A-2. In the experiment, the voltage signal delivered by the amplifier was not stable enough. So, batteries and resistors described by Siddiquee (23) were used as the amplifier.

Installation and operation of the whole data logging system are explained in great detail in the user's guide (43,44,45).

PIN 8...CHANNEL 1+

PIN 7...CHANNEL 2+

PIN 6...CHANNEL 0+

PIN 5...CHANNEL 3+

PIN 4...GROUND

PIN 3...GUARD

PIN 2...OUTPUT D

PIN 1...OUTPUT A

PIN 15...CHANNEL 1-

PIN 14...CHANNEL 2-

PIN 13...CHANNEL 0-

PIN 12...CHANNEL 3-

PIN 11...DIGITAL INPUT

PIN 10...OUTPUT C

PIN 9 ...OUTPUT B

Table A-1. Connector Pinout of Digital Board

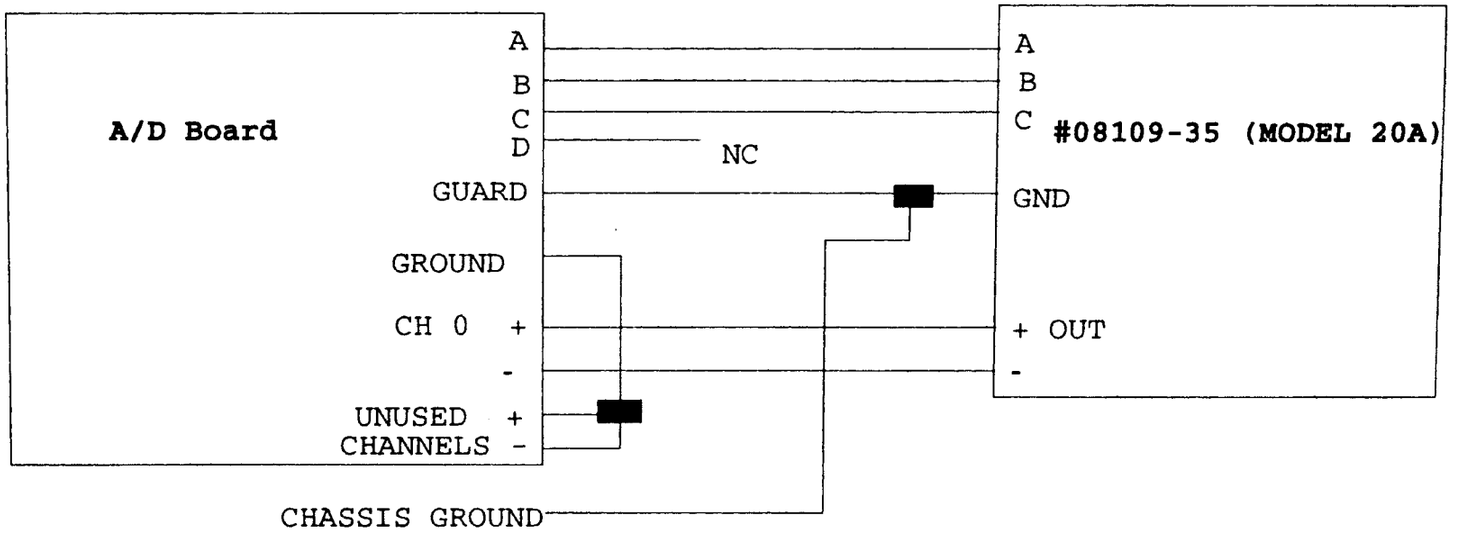

Figure A-2. Interconnection Diagram For
#08109-35 (MODEL 20A)

APPENDIX B

VIDEO IMAGE TECHNIQUE

Video image processing and digitizing technique were used to quantify the extensional flow-induced crystallization in the experimental work. Pixel values were measured and plotted as a function of time. Pixels are the elements of video image. In a black and white video system, each pixel is given an integer value ranging from 0 to 255 called gray value. A gray value of 0 correspond to a complete darkness while a value of 255 corresponds to a complete white element. Pixel value is not the same as the intensity of light, but it reflects the trend of intensity of light. The calibration technique was presented by Tree (1).

A DT2853 Frame Grabber (already installed in the computer) was used to convert the intensity of light to a pixel value by connecting VCR, monitor and computer correctly. The wiring connections are shown in Figure B-1 and Figure B-2. Once all the connections are secured properly, replay the video tape frame by frame so that the IRIStutor Image Processing Software can be used to obtained the pixel value. By using IRIStutor,video images digitized by DT2853 could be acquired, stored and retrieved without writing a program. The IRIStutor was executed by typing "IR" followed by a carriage return in "IRIS-t" sub-directory under DOS prompt. By typing the following IRIStutor commands, pixel value at any position of the image:

COMMAND: SYNC EXTERNAL

COMMAND: DISPLAY CAMERA

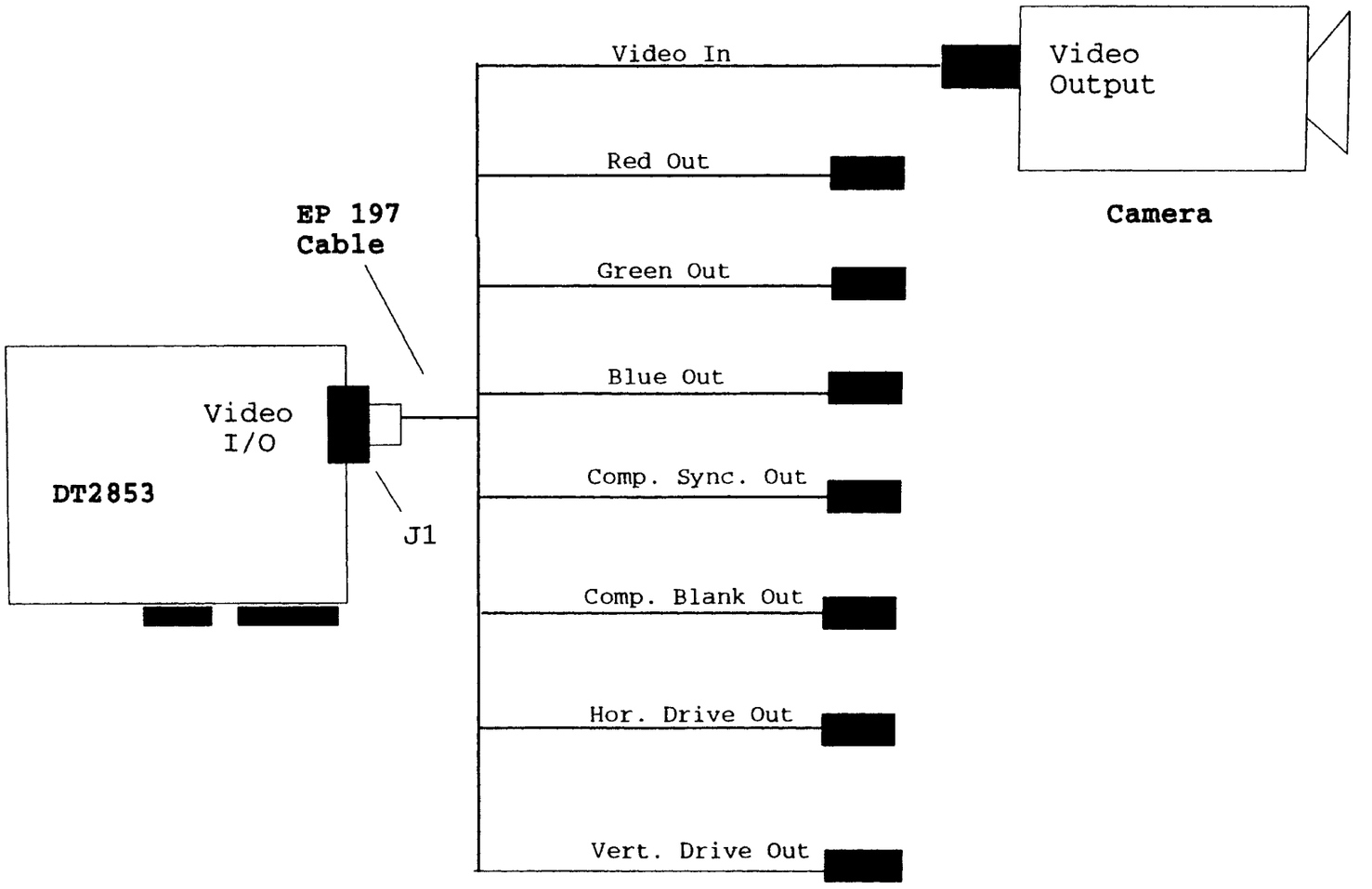

Figure B-1. Wiring Connection of VCR and Computor

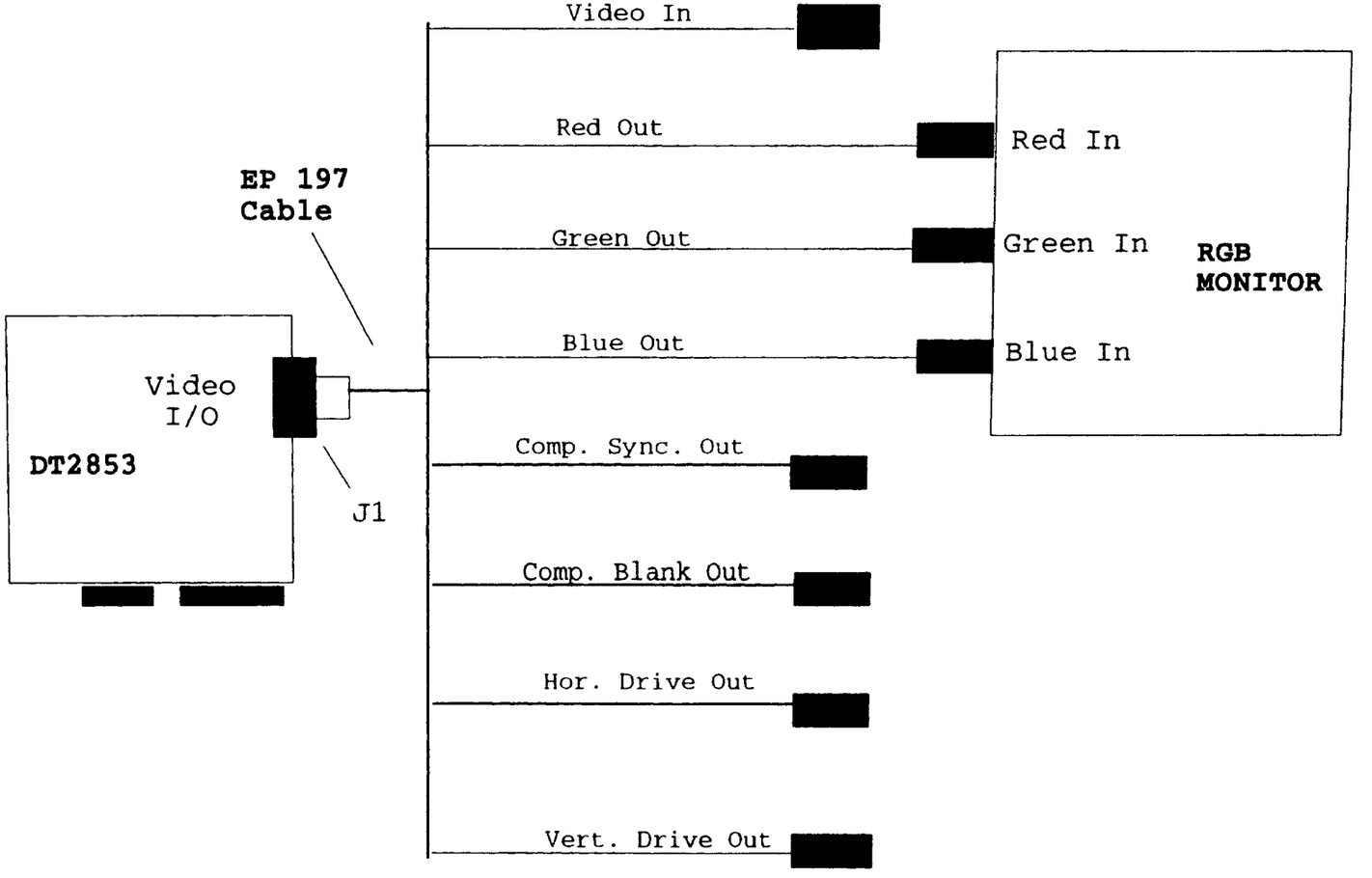

Figure B-2. Wiring Connection of Monitor and Computer

COMMAND: PLACE_CURSOR

DT2853 User Manual (46) gives more detailed description about all the IRIStutor commands and the whole system setup and operation.

APPENDIX C

COMPUMOTOR

The computer controlled motor and X-Language used in the experiment were explained in great detail by Siddiquee (23), the User Guide (47) and Software Reference Guide (48). However, the pins two, three and nine are Rx, Tx and the ground when the indexer was connected to the computer via RS 232c interface is incorrect. It should be pins two, three and seven.

APPENDIX D

CALIBRATION OF DATA LOGGING SYSTEM

To calibrate the data logging system, following procedure should be used:

1. From the "C>" prompt, type "LOG_SRCA" followed by a carriage return to run the program.

2. Select "Configure System" from the main menu and press carriage return.

3. Select "define the data point" from the configuration menu and press carriage return.

4. Make sure the readings from screen look like the following:

a. Input Channel ---------- 0

b. External Device ---------- Multiplexer

c. External Device Channel ---------- 0

5. Set the offset factor equal to zero and the scaling factor equal to 1 on the screen.

6. Set the torque meter at the zero position on the stationary cylindrical dial.

7. Read the digital value (corresponding to torque value of zero) from the "Formatted reading" on the screen. The digital value is equivalent to the voltage value in the built-in potentiometer of the torque meter.

8. Set the torque meter to the 0.5 in-lb position on the dial.

9. Read the digital value corresponding to a torque value of 0.5 in-lb.

10. Repeat steps (8) and (9) with the torque meter set at 1.0, 1.5, 2.0 in-lb.

11. Plot the digital value vs. torque data in X-Y coordinates (linear relationship).

12. Read the value of the intercept and the slope from the plot.

13. Set the offset factor equal to the intercept and the scaling factor equal to the slope on the screen.

14. Adjust the torque meter to a different position on the dial. If the values from "Formatted Reading" on the screen are equal to the torque value on the cylindrical dial on the torque meter, the calibration is correct. If not, repeat steps 4 to 13.

APPENDIX E

EXPERIMENTAL RESULTS

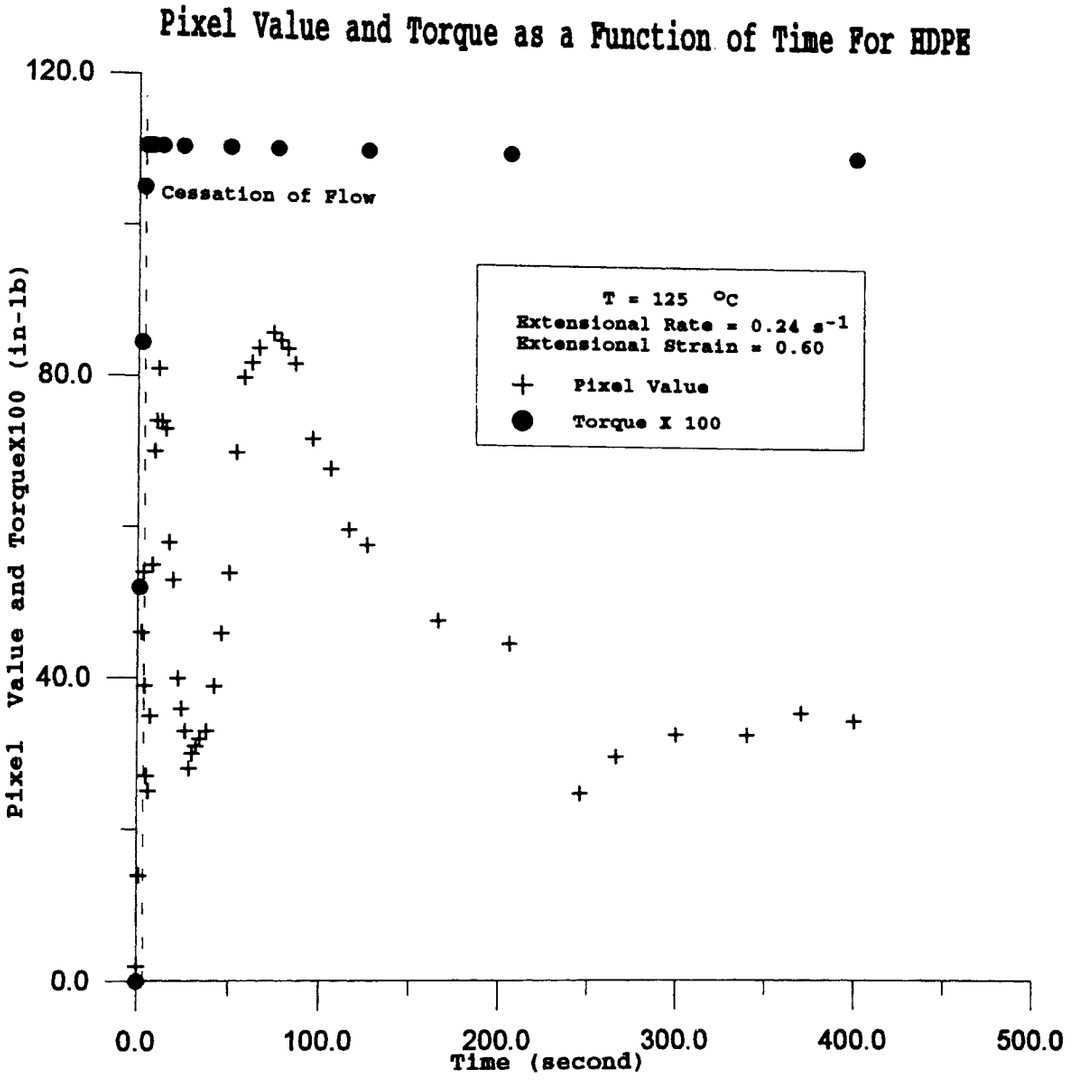

Figure E-1. Pixel value and Torque as a Function of Time

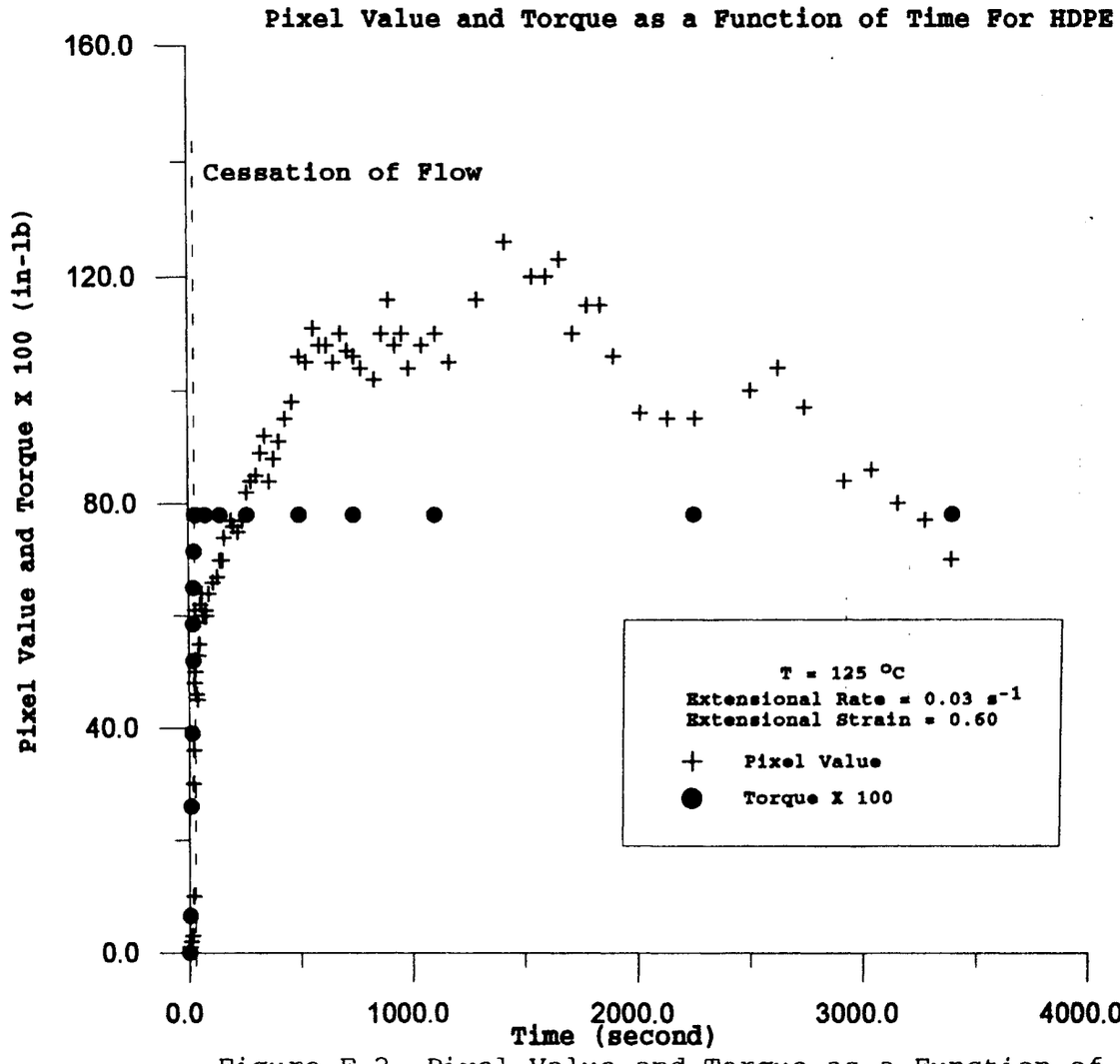

Figure E-2. Pixel Value and Torque as a Function of Time

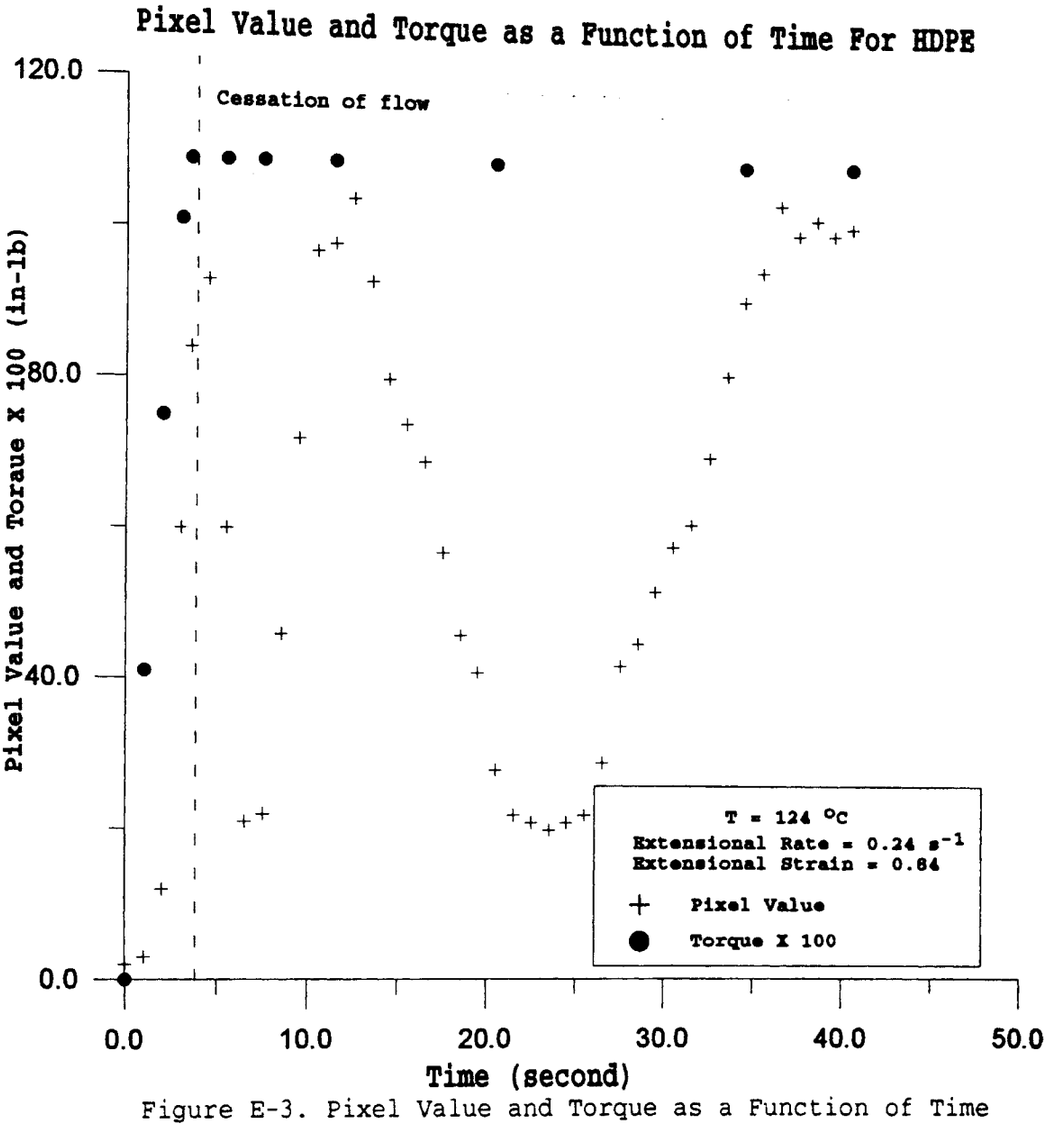

Figure E-3. Pixel Value and Torque as a Function of Time

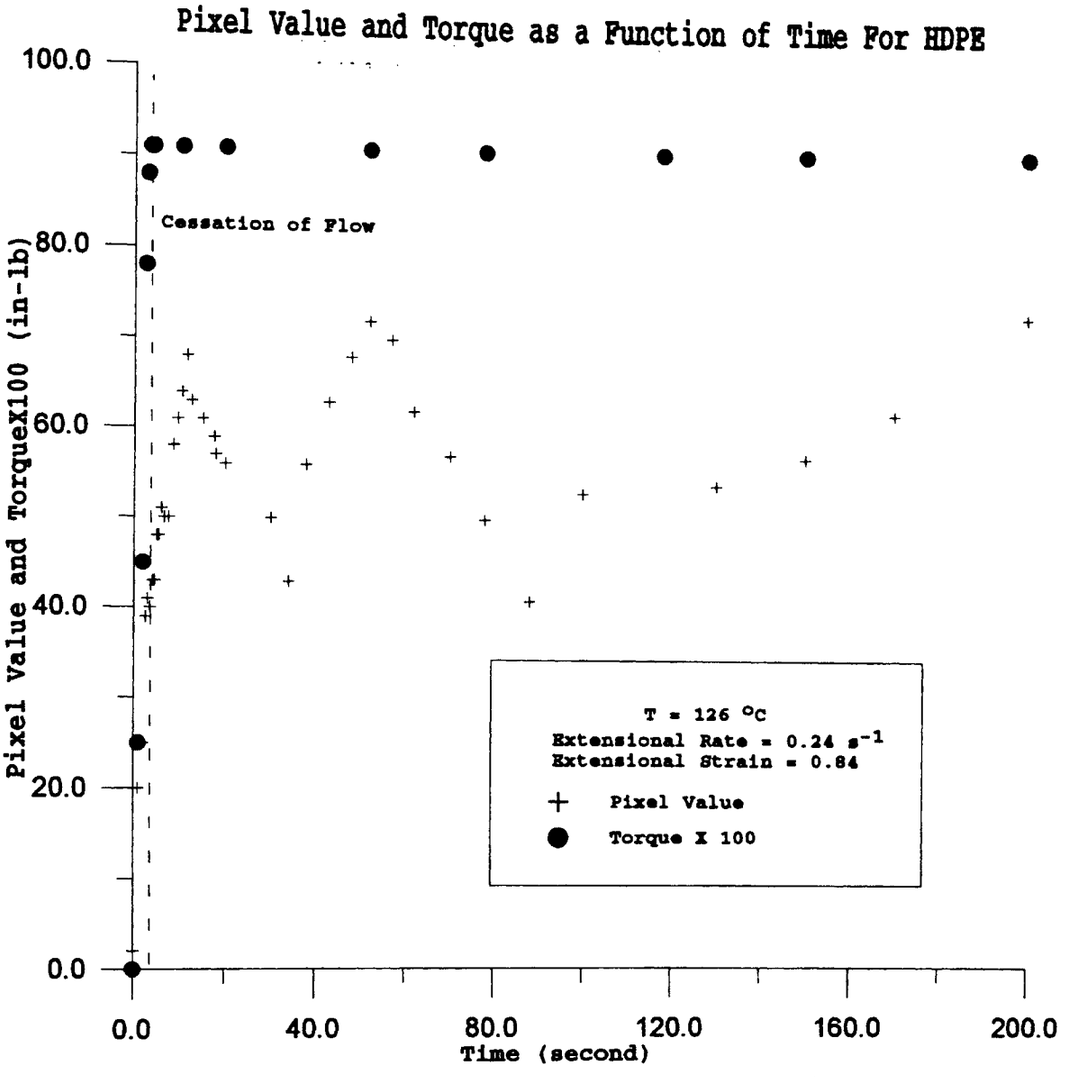

Figure E-4. Pixel Value and Torque as a Function of Time

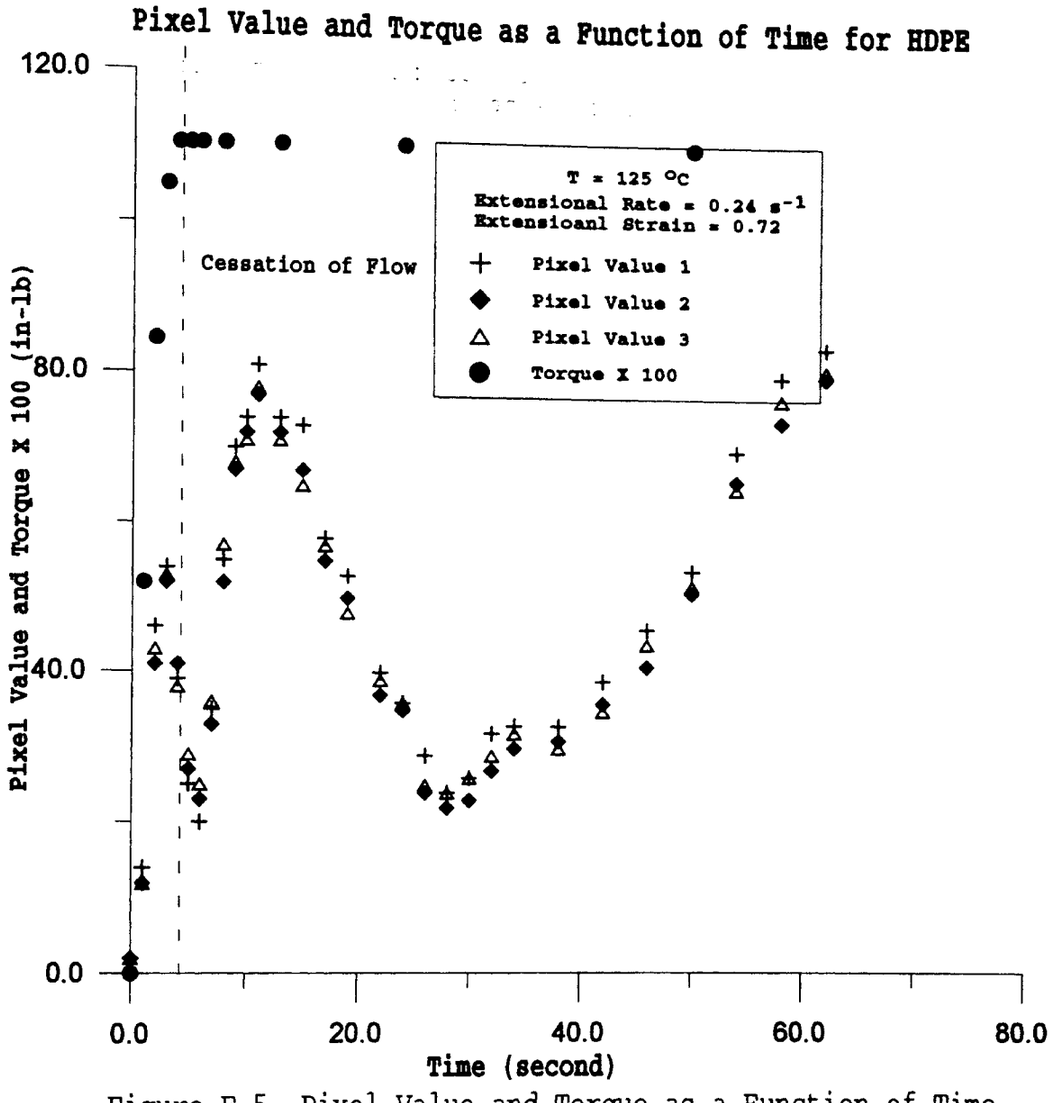

Figure E-5. Pixel Value and Torque as a Function of Time

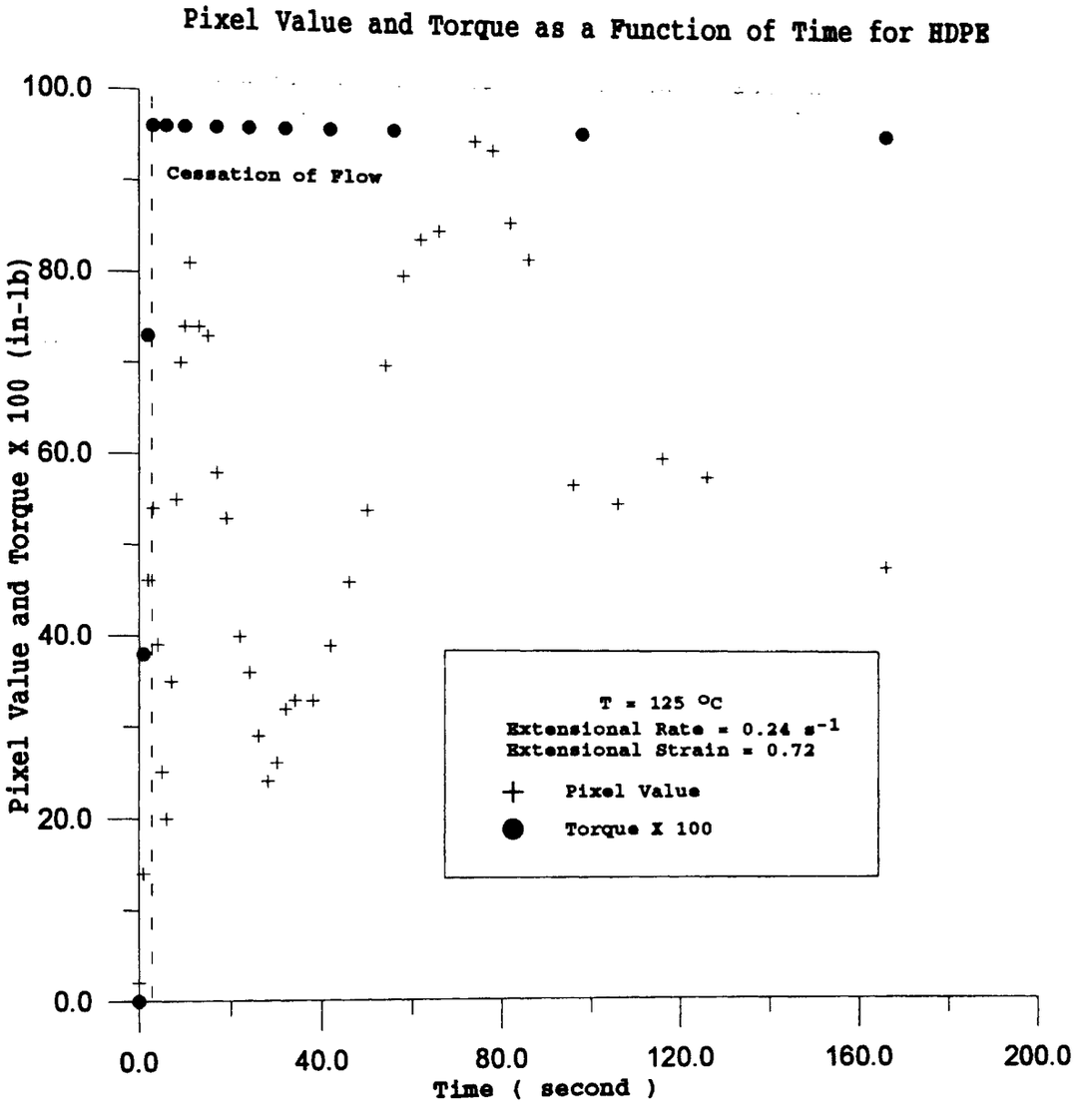

Figure E-6. Pixel Value and Torque as a Function of Time

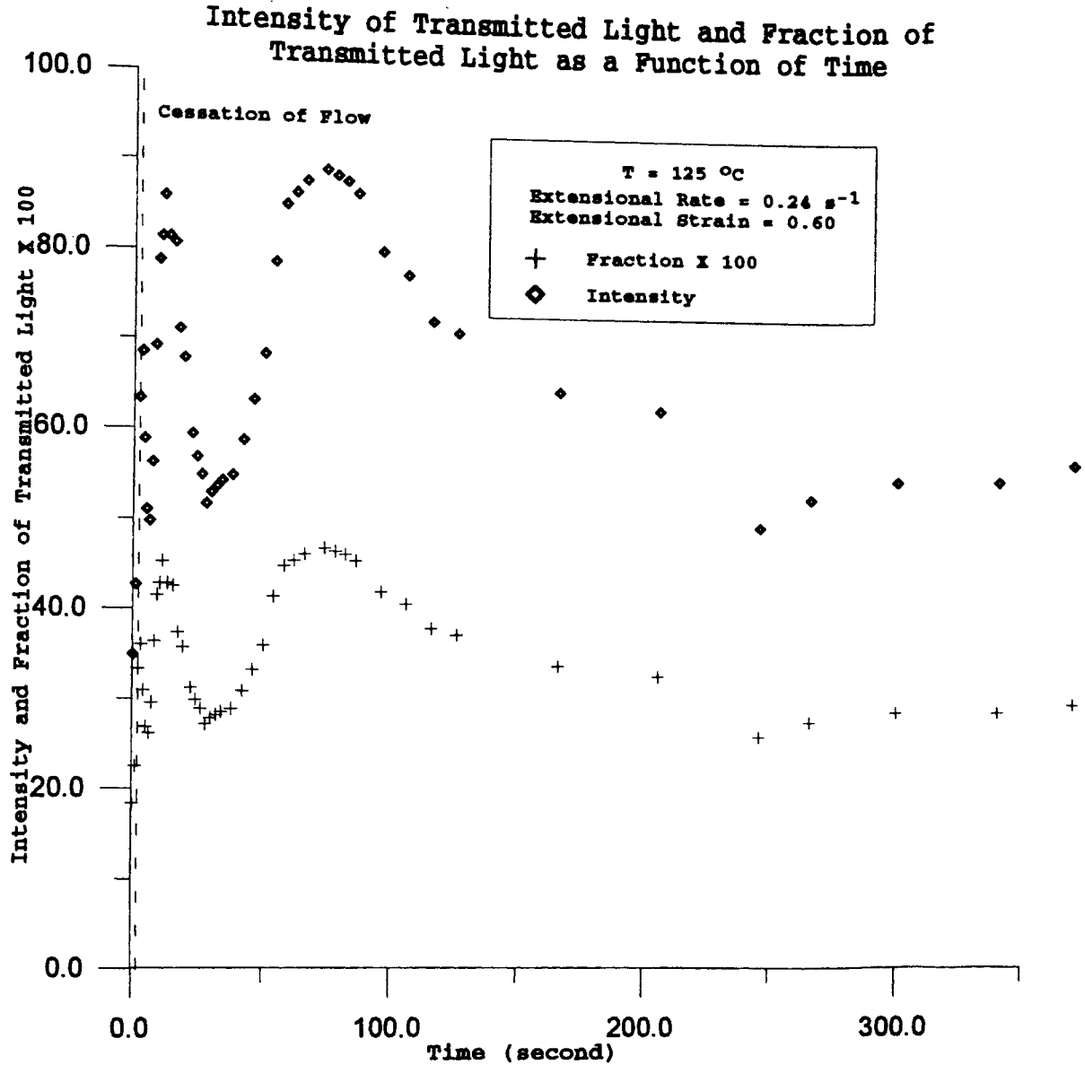

Figure E-7. Intensity of Transmitted Light and Fraction of Transmitted Light as a Function of Time

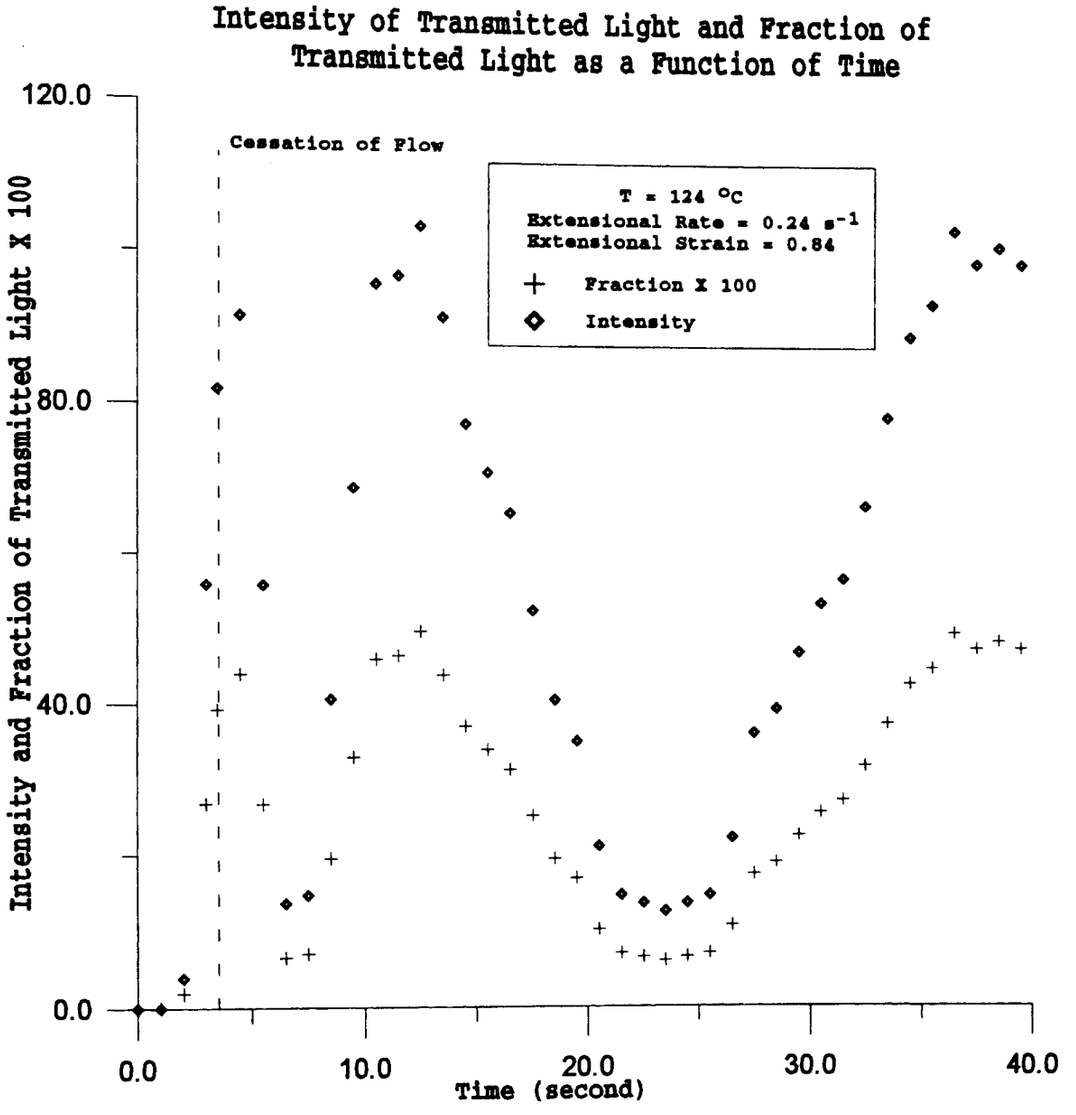

Figure E-8. Intensity of Transmitted Light and Fraction of Transmitted Light as a Function of Time

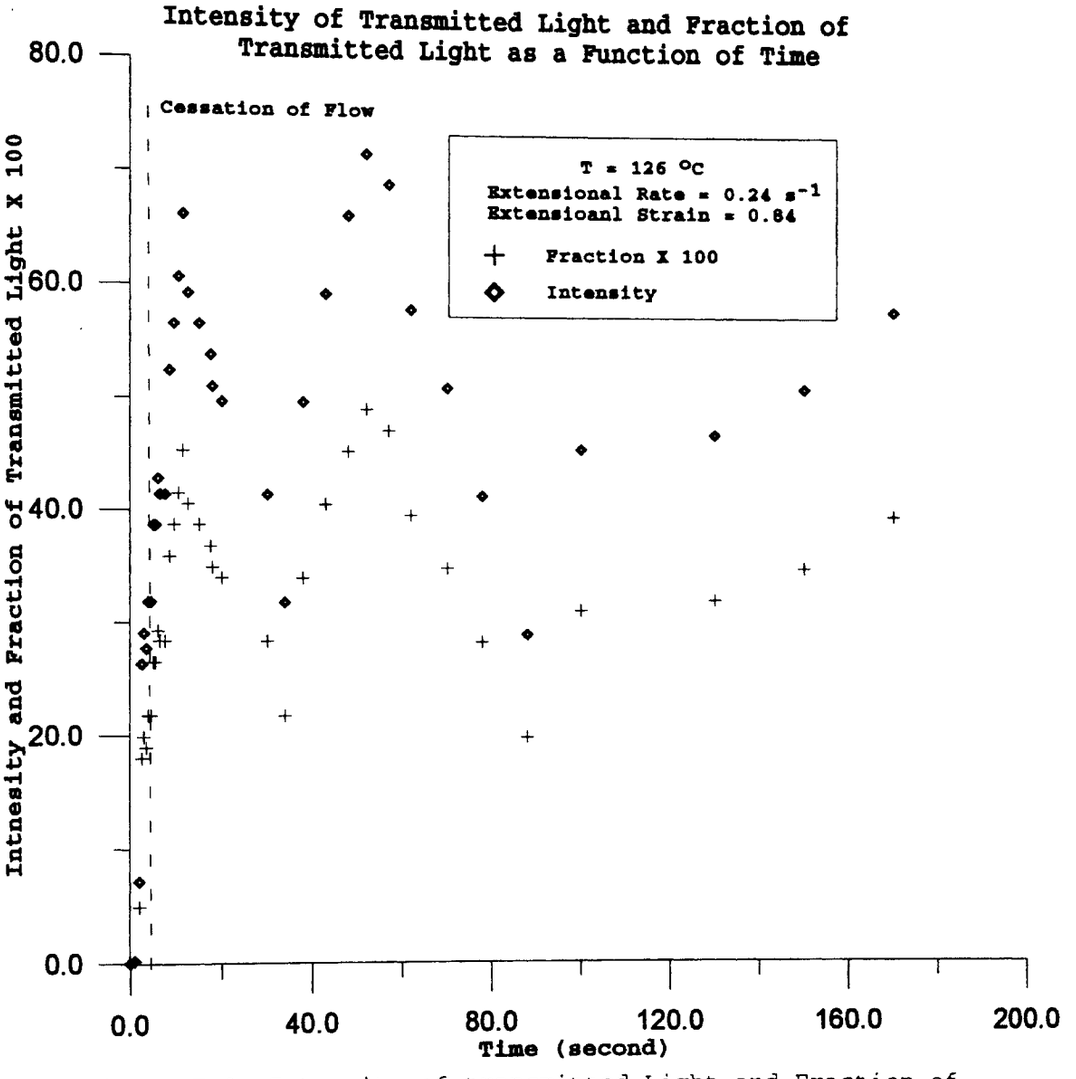

Figure E-9. Intensity of transmitted Light and Fraction of Transmitted Light as a Function of Time

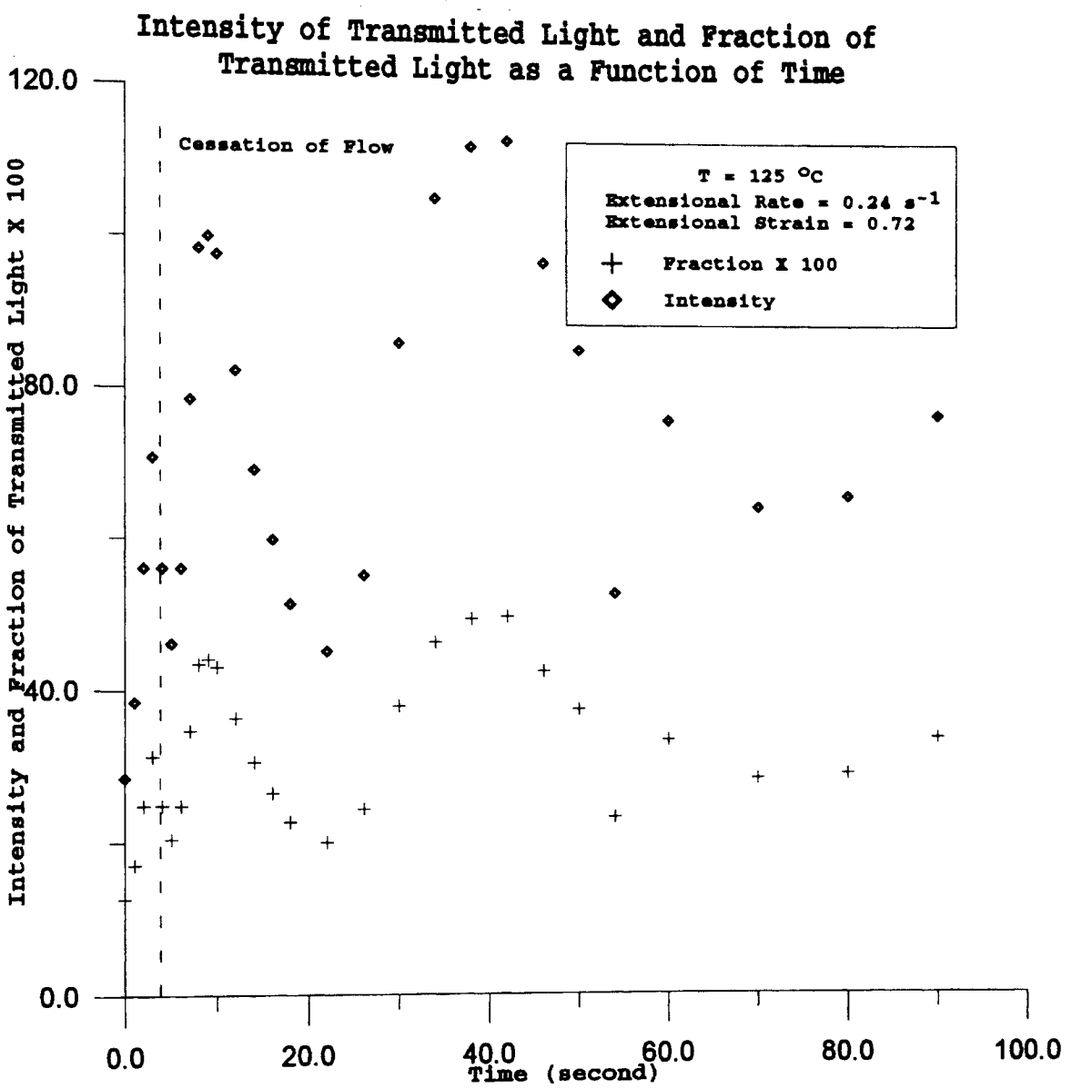

Figure E-10. Intensity of Transmitted Light and Fraction of Transmitted Light as a Function of Time

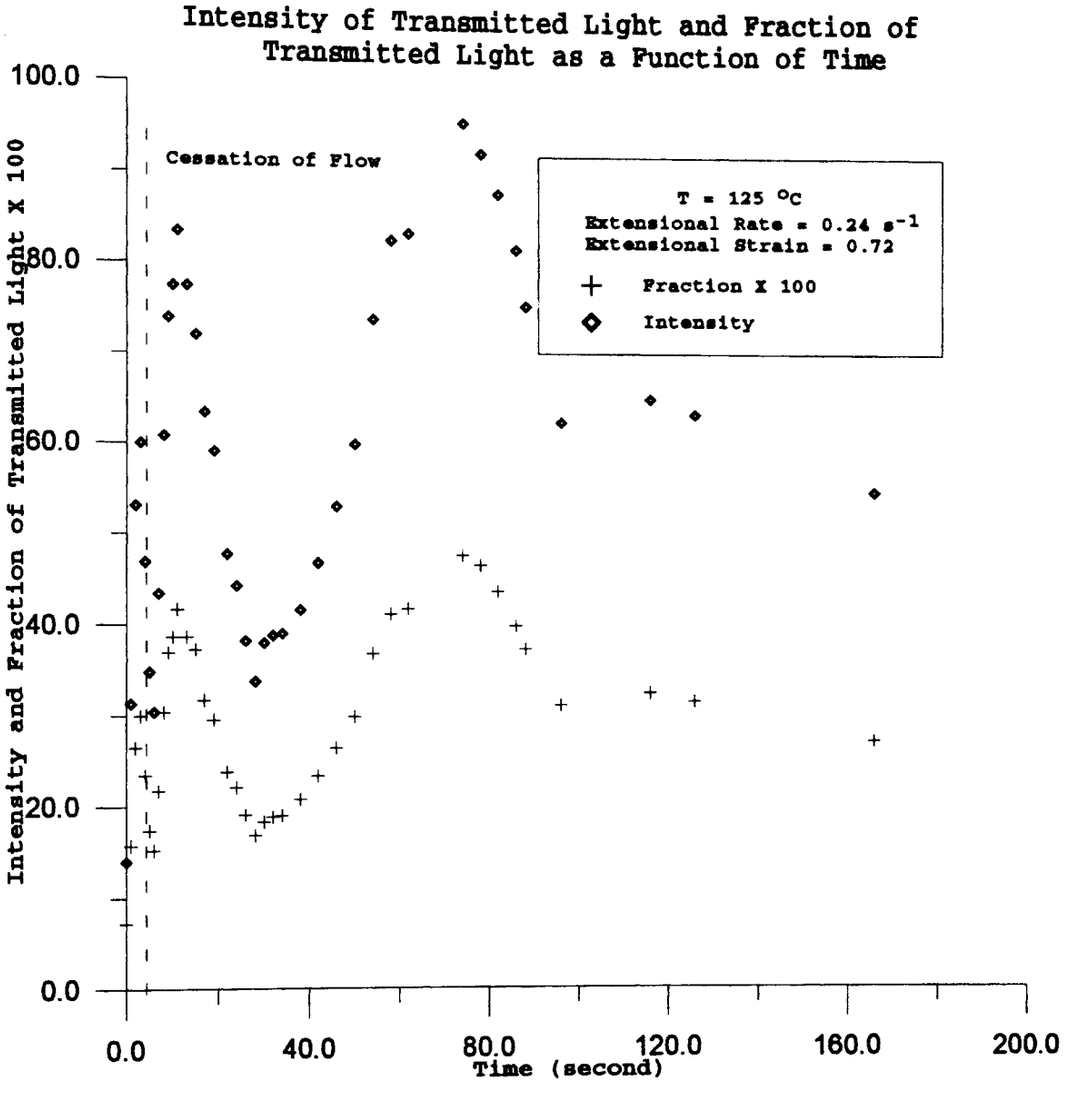

Figure E-11. Intensity of Transmitted Light and Fraction of Transmitted Light as a Function of Time

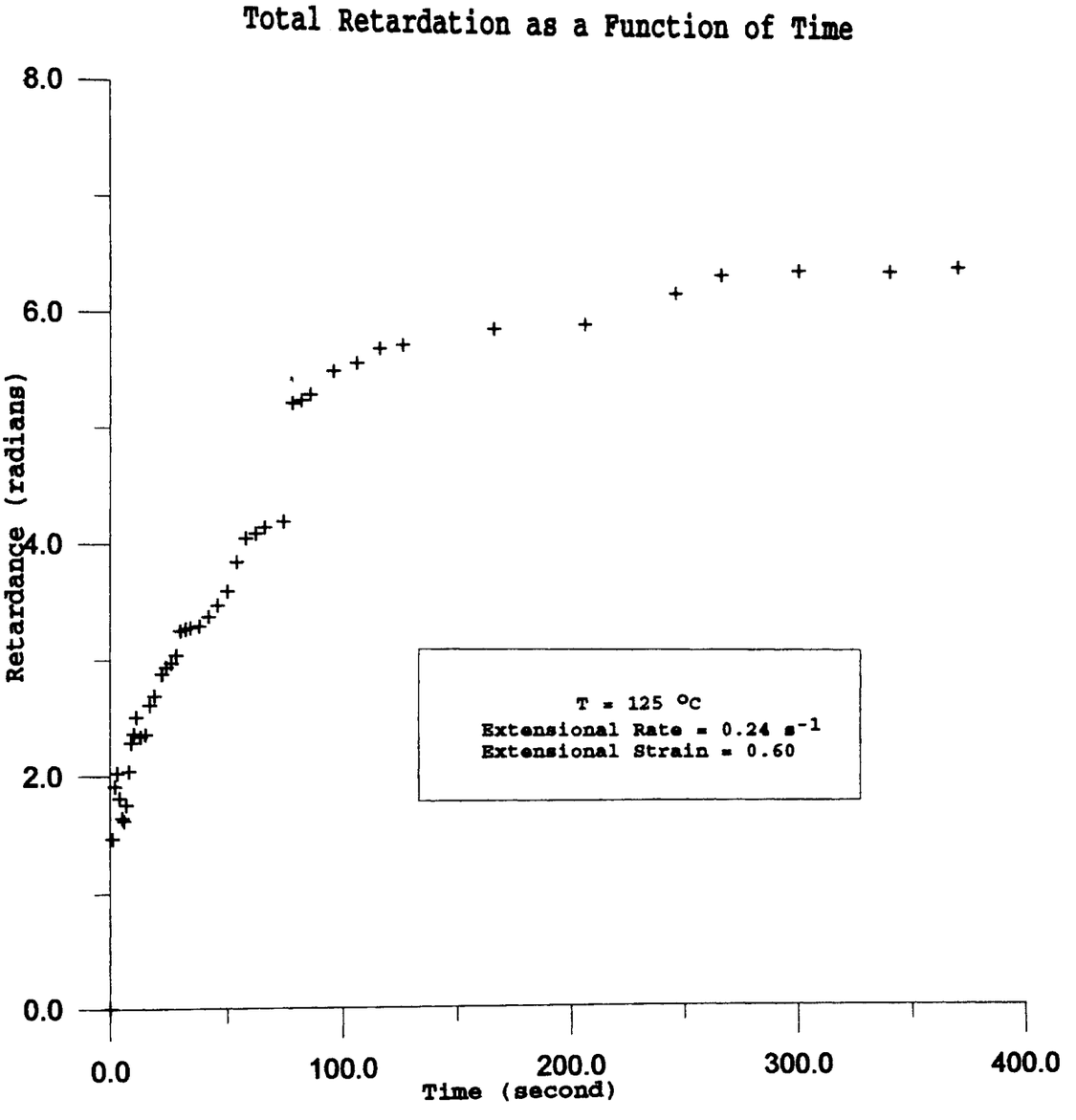

Figure E-12. Retardance as a Function of Time

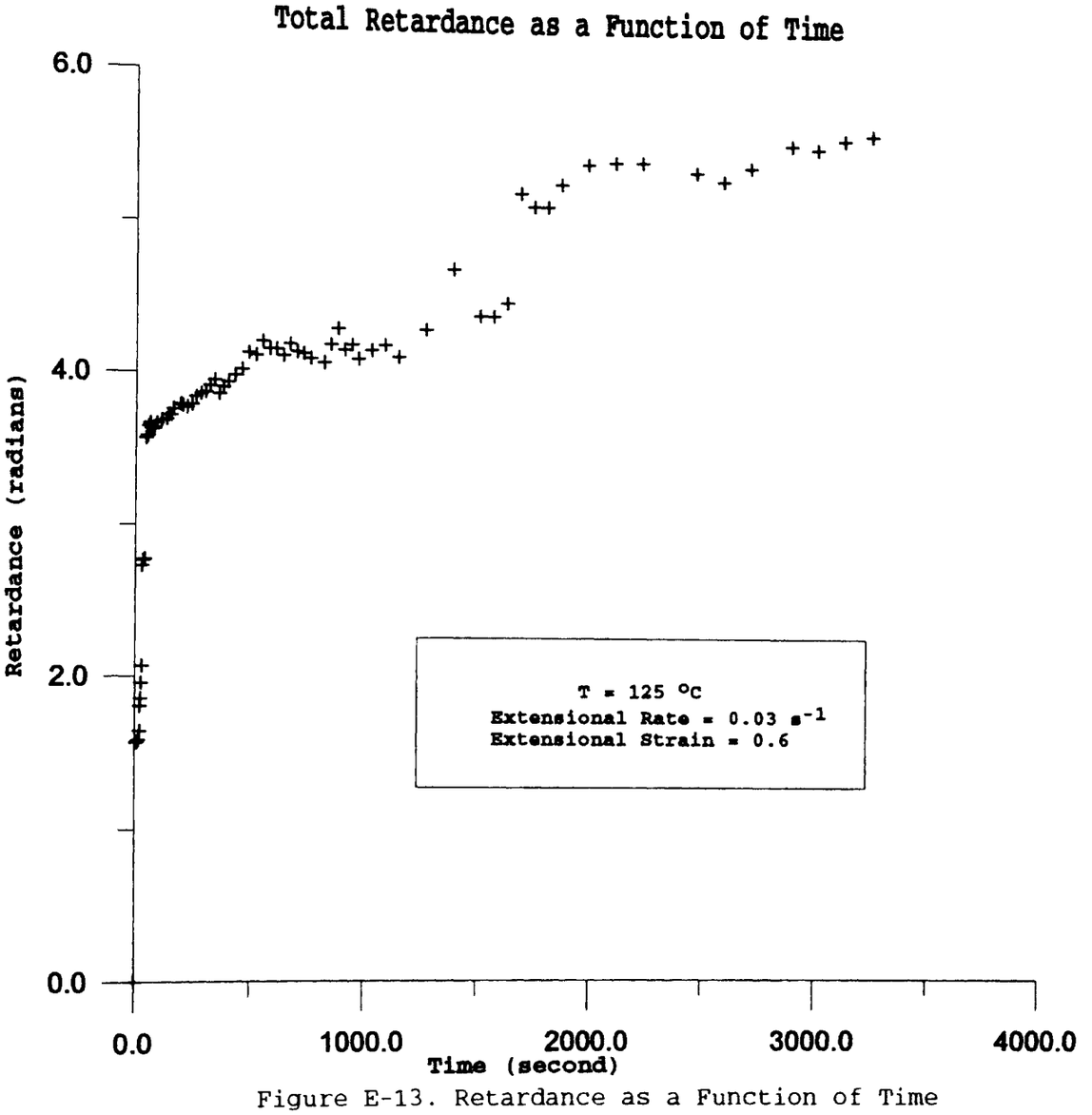

Figure E-13. Retardance as a Function of Time

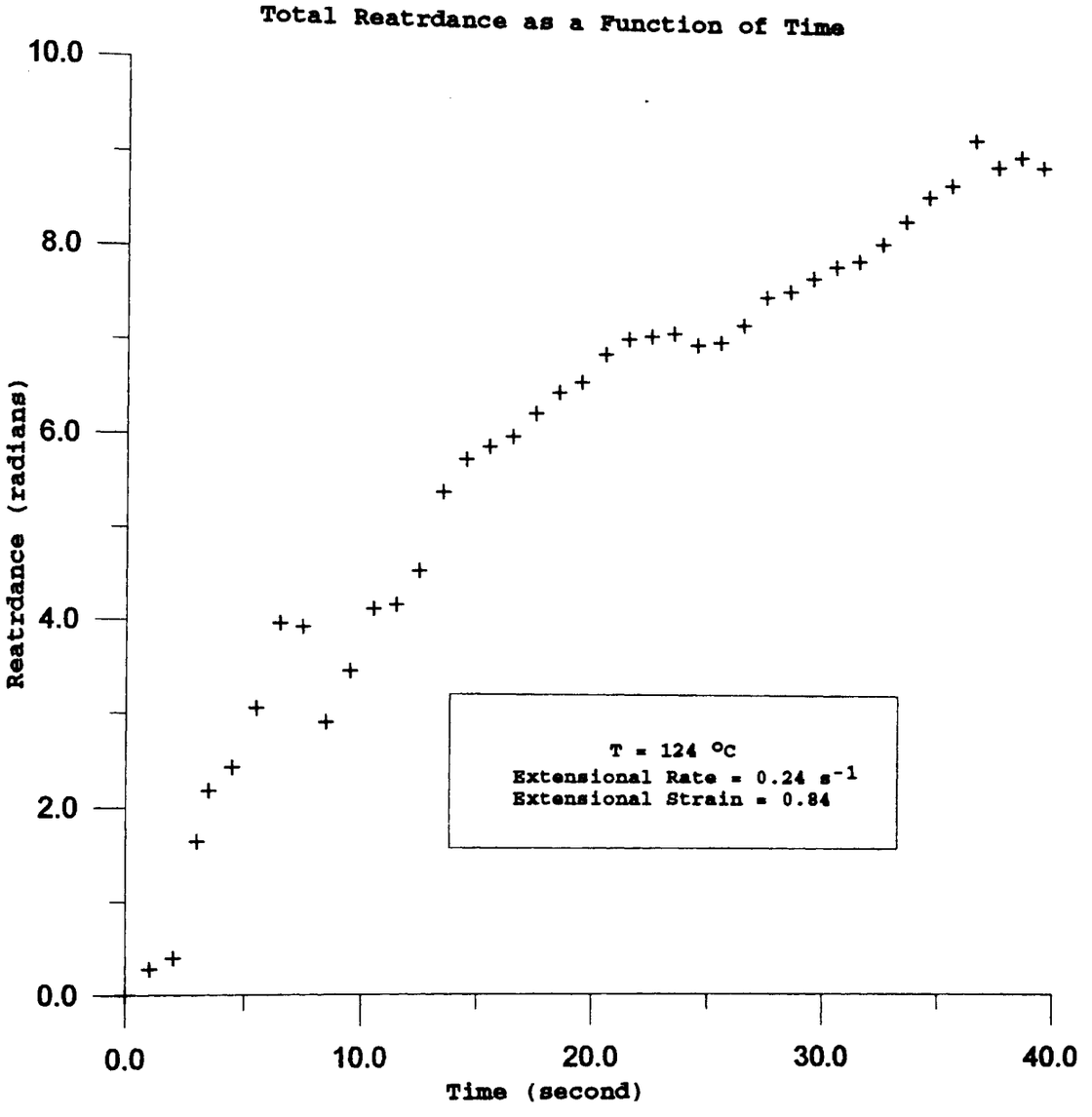

Figure E-14. Retardance as a Function of Time

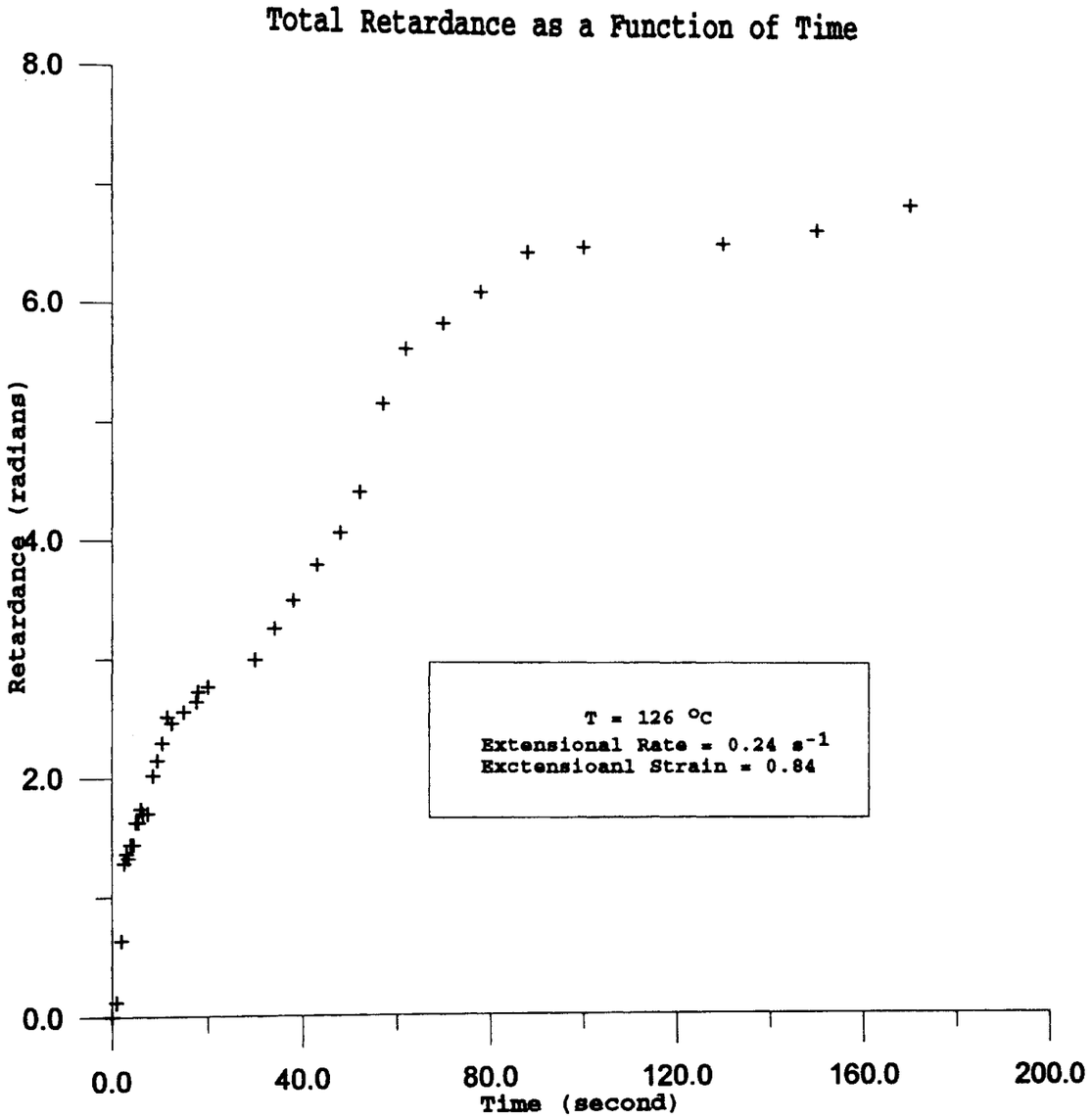

Figure E-15. Retardance as a Function of Time

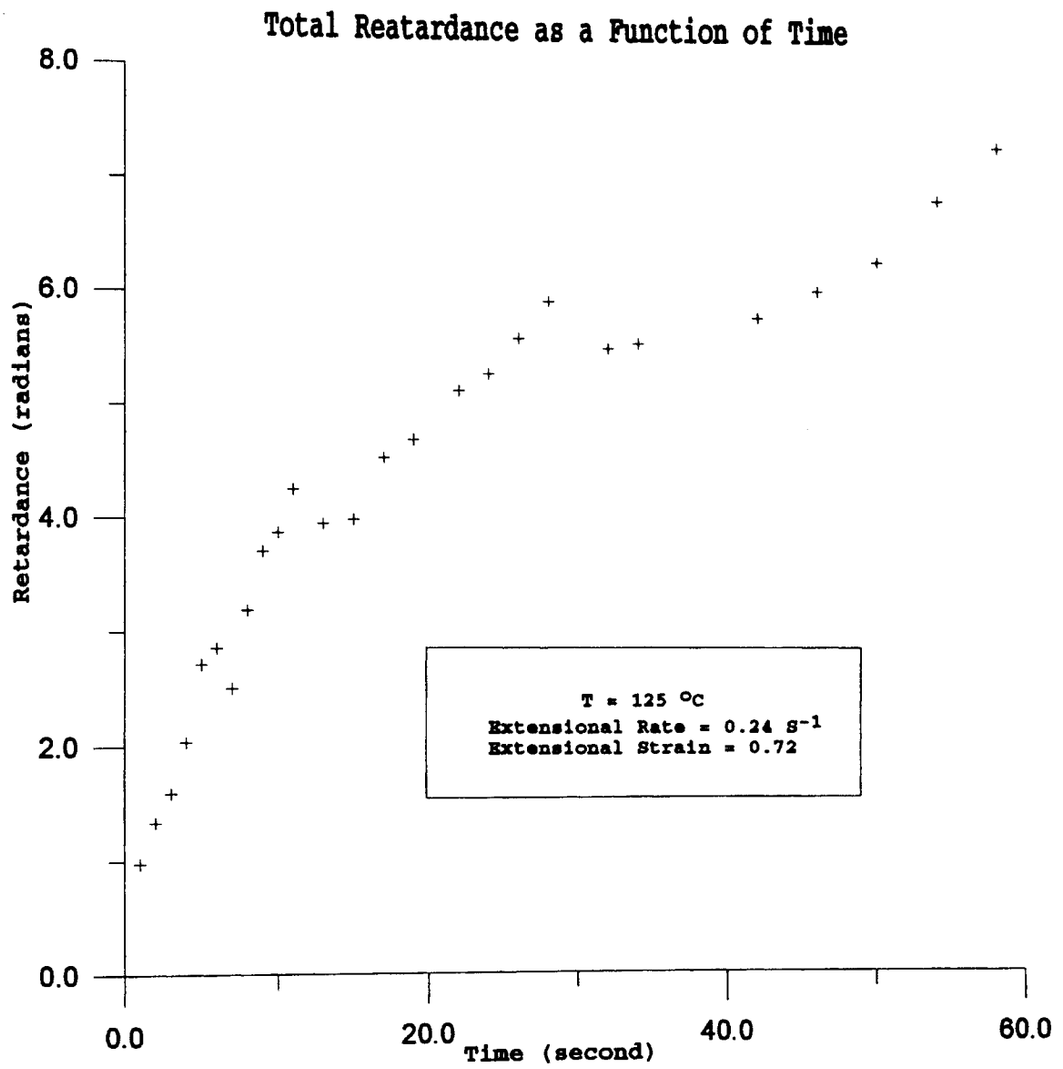

Figure E-16. Retardance as a Function of Time

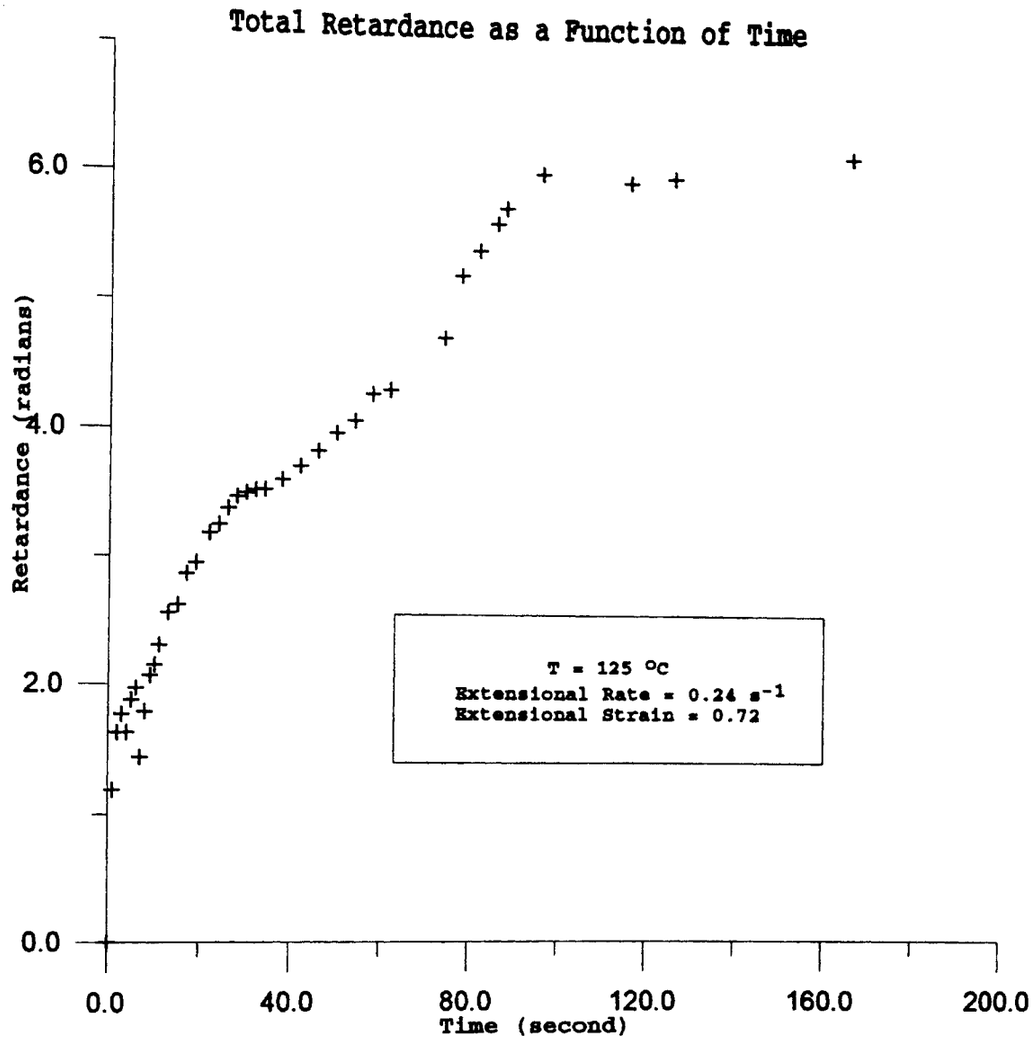

Figure E-17. Retardance as a Function of Time

VITA

Sheng Ma

Candidate for the Degree of

Master of Science

Thesis: THE CRYSTALLIZATION KINETICS OF POLYETHYLENE IN EXTENSIONAL DEFORMATION

Major Field: Chemical Engineering

Biographical:

Personal Data: Born in Hangzhou, P.R. of China, October 18, 1968, the son of Shen-xian Ma and Feng-cai Han.

Education: Graduated from Number 15 Hangzhou High School, Hangzhou, P.R. of China June 1986; received Bachelor of Science Degree in Chemical Engineering from Zhejiang University at Hangzhou in June, 1990; completed requirements for the Master of Science degree at Oklahoma State University in December, 1994.

Personal Experience: Assistant Engineer, Department of Chemical Engineering, Zhejiang University,July 1990, to July 1992. Teaching Assistant, School of Chemical Engineering, Oklahoma State University, August, 1992, to December, 1993. Research Assistant, School of Chemical Engineering, Oklahoma State University, January, 1994, to December, 1994.